2019

Vortex Induced Convective Heat Transfer Augmentation

Junguo Wang
University of Windsor

Vortex Induced Convective Heat Transfer Augmentation

By

Junguo Wang

A Thesis
Submitted to the Faculty of Graduate Studies
through the Department of Mechanical, Automotive, and Materials Engineering
in Partial Fulfillment of the Requirements for
the Degree of Master of Applied Science
at the University of Windsor

Windsor, Ontario, Canada

2019

Vortex Induced Convective Heat Transfer Augmentation

by

Junguo Wang

APPROVED BY:

_____

S. Ray
Essex Energy Corporation

_____

R. Carriveau
Department of Civil and Environmental Engineering

_____

V. Stoilov
Department of Mechanical, Automotive, and Materials Engineering

_____

D. S-K. Ting, Advisor
Department of Mechanical, Automotive, and Materials Engineering

March 28, 2019

DECLARATION OF ORIGINALITY

I hereby certify that I am the sole author of this thesis and that no part of this thesis has been published or submitted for publication.

I certify that, to the best of my knowledge, my thesis does not infringe upon anyone's copyright nor violate any proprietary rights and that any ideas, techniques, quotations, or any other material from the work of other people included in my thesis, published or otherwise, are fully acknowledged in accordance with the standard referencing practices. Furthermore, to the extent that I have included copyrighted material that surpasses the bounds of fair dealing within the meaning of the Canada Copyright Act, I certify that I have obtained a written permission from the copyright owner(s) to include such material(s) in my thesis and have included copies of such copyright clearances to my appendix.

I declare that this is a true copy of my thesis, including any final revisions, as approved by my thesis committee and the Graduate Studies office, and that this thesis has not been submitted for a higher degree to any other University or Institution.

ABSTRACT

Delta winglet is an effective means to passively augment heat convection from a hot surface such as a solar panel. The effects of an inclination angle on the flow downstream of the winglet were studied. A delta winglet with an aspect ratio (c/h) of 2 and an attack angle of 30 degrees was mounted on a flat plate to scrutinize the role of its inclination angle (90° and 120°) on the flow downstream. The inclined winglet was placed in a wind tunnel, and the flow was measured by the hotwire. The experiment shows the 120-degree-inclination-angle delta winglet can generate an inflow velocity larger than 90 degrees. The heat transfer enhancement caused by the delta winglet was then investigated. Three different inclination angles (60°, 90° and 120°) of the delta winglet were studied, and a thermal camera was used to maintain the heat transfer enhancement of the heated panel. The result shows that the delta winglet with the inclination angle of 120 degrees can generate the best thermal performance.

DEDICATION

To family

ACKNOWLEDGEMENTS

First, I would like to thank Dr. David S-K. Ting for his scrupulous supervision throughout my MASc pursuit. I want to thank Mr. Steve Ray for his meticulous support on this project. I am most grateful to Dr. Carriveau and Dr. Stoilov for providing valuable suggestions which drastically improve this thesis.

This work was made possible by Natural Sciences and Engineering Research Council of Canada and Ontario Centres of Excellence.

TABLE OF CONTENTS

LIST OF FIGURES

LIST OF APPENDICES

CHAPTER 1

INTRODUCTION

1.1 Motivation and Background

The ultimate goal of this research is to study the cooling of a solar panel. In previous studies, it has been found that the higher the cell temperature of a solar photovoltaic (PV) solar panel, the lower the efficiency. So, it is essential to study the cooling of the solar panel to enhance the efficiency of the PV panel. There are two requirements of the cooling method, one is to enhance the heat transfer rate efficiently, and the other is that the means should not block the solar radiation which can decrease energy absorbed by the solar panel.

Vortex generators punched out from the surface is one of the commonly used methods to enhance the heat transfer rate of the surface by generating turbulence and vortices in the flow. The heat transfer rate is controlled by the secondary flow, turbulence caused by the vortex generators. Many kinds of turbulent generators (TG) have been applied to enhance heat transfer via the resulting flow turbulence and vorticity [1,2]. These vortex generators may include longitude vortex generators [3,4], ribs [5], or dimples [6]. These vortex generators are widely used in many industrial applications including the cooling of electronics, heat exchangers, and cooling of solar panels, which can enhance the efficiency of the application.

Delta winglet is a passive turbulent generator (TG) which tends to generate a longitude vortex capable of penetrating the turbulent boundary layer [7]. The longitude vortex is a kind of long-lasting vortex which can exist in a long stream-wise distance. In engineering, delta winglet is a promising longitude vortex generator which can generate

longitude vortex and high-intensity turbulence to enhance the heat transfer rate effectively. Previous researchers found that the delta winglet has the best performance among all longitude vortex generators [8]. Many studies have been carried on the heat transfer augmentation caused by the delta winglet in the heat exchanger. To investigate the heat transfer enhancement caused by the delta winglet, this research was performed in the wind tunnel which can be considered as an unconfined flow.

1.2 Thesis Objective and Overview

The objective of this paper is to find the most effective way to enhance convective heat transfer rate of the solar panel and explain the augmentation in terms of the altered flow field characteristic. To achieve the objective, the turbulent flow structure and vortex intensity of longitudinal vortex were qualified under different inclination angles (60°, 90° and 120°) with a fixed attack angle of 30° and aspect ratio of 2 to investigate the influence of turbulent vortical flow on the Nusselt number on the PTFE plate. The flow was measured by a 3D hotwire. The heat transfer enhancement was evaluated by using a thermal camera and thermal couples. The procedure of the research was presented as follows:

Chapter 1 (Introduction)

The motivation, background and the objective of the research.

Chapter 2

In this part, the effect of the inclination angle of a delta winglet vortex generator with a length-to-height (c/h) ratio of 2, at 30 degrees with respect to a Re_h = 9000 wind, on the resulting flow along a flat plate was quantified in a wind tunnel. The vortical flow

characteristics at 13h downstream of the leading edge of the delta winglet were detailed with the help of a triple-hot-wire probe. Specifically, the local velocity, vortex shape, size and strength, turbulence intensity, integral length, and Taylor microscale were deduced. The results show that the into-the-plate velocity in the inflow region increased, while the out-of-the-plate velocity in the outflow area decreased, with the increasing of the inclination angle. The 90-degree inclination angle appears to furnish higher values of turbulent intensity, integral length, and Taylor microscale.

Chapter 3

As next step, a delta winglet (DW) with an aspect ratio (c/h) of 2 and an attack angle of 30 degrees was mounted on a heated flat plate to scrutinize the role of its inclination angle (60°, 90° and 120°) on convection heat transfer enhancement. The experiment was conducted at a Reynolds number, Re_h, of 6300 in a wind tunnel. The heat transfer enhancement deduced from a thermal camera was expressed in terms of Nusselt number normalized by the reference no-winglet case for the streamwise distance from 0 to 16h. It was found that the largest tested inclination angle of 120° resulted in the most heat transfer enhancement. The results were explained in terms of the vortical flow characteristics detailed at 13h, where the most substantial downwash velocity and affected area were obtained for the 120° inclination angle case. This vertical downwash caused a larger enhancement than the slightly more considerable turbulent kinetic energy produced by the 90° inclination angle winglet.

Chapter 4 (Conclusion)

In the last chapter, a conclusion and summary were made with respect to the results of the whole research. Moreover, a possible direction of the future work was raised in this chapter.

Appendix

Uncertainty analysis of the experiment. And the publication status.

References

[1] Jindal, P., Agarwal, S., Sharma, R. P., and Roy, A. K., 2018, "Enhancement of Film Cooling Effectiveness Using Rectangular Winglet Pair," Journal of Thermal Science and Engineering Applications, **10**(4), pp. 041014-041014–9.

[2] Agarwal, S., and Sharma, R. P., 2016, "Numerical Investigation of Heat Transfer Enhancement Using Hybrid Vortex Generator Arrays in Fin-and-Tube Heat Exchangers," Journal of Thermal Science and Engineering Applications, **8**(3), pp. 031007-031007–9.

[3] Li, J., Dang, C., and Hihara, E., 2019, "Heat Transfer Enhancement in a Parallel, Finless Heat Exchanger Using a Longitudinal Vortex Generator, Part B: Experimental Investigation on the Performance of Finless and Fin-Tube Heat Exchangers," International Journal of Heat and Mass Transfer, **128**, pp. 66–75.

[4] Li, J., Dang, C., and Hihara, E., 2019, "Heat Transfer Enhancement in a Parallel, Finless Heat Exchanger Using a Longitudinal Vortex Generator, Part A: Numerical Investigation," International Journal of Heat and Mass Transfer, **128**, pp. 87–97.

[5] Rezazadeh, R., Pourmahmoud, N., and Asaadi, S., 2018, "Numerical Investigation and Performance Analyses of Rectangular Mini Channel with Different Types of Ribs and Their Arrangements," International Journal of Thermal Sciences, **132**(Complete), pp. 76–85.

[6] Chimres, N., Wang, C.-C., and Wongwises, S., 2018, "Optimal Design of the Semi-Dimple Vortex Generator in the Fin and Tube Heat Exchanger," International Journal of Heat and Mass Transfer, **120**, pp. 1173–1186.

[7] R. L. Webb and N. Kim, "Enhanced Heat Transfer," Taylor and Francis, New York, 1994.

[8] Mitra, N., Fiebig, M., and others, 1994, "Comparison of Wing-Type Vortex Generators for Heat Transfer Enhancement in Channel Flows," Journal of heat transfer, **116**(4), pp. 880–885.

CHAPTER 2

THE EFFECT OF DELTA WINGLET INCLINATION ANGLE ON THE VORTICAL FLOW DOWNSTREAM

2.1 Introduction

Delta winglet is a passive turbulent generator (TG) which tends to generate a longitude vortex which can penetrate into the turbulent boundary layer [1]. It is widely used in many engineering applications such as heat exchangers [2, 3], and the induced turbulence under various conditions is also of fundamental interest.

Eibeck and Eaton [4] studied the structure of the longitude vortex created by the delta winglet at different downstream locations in 1987. Their work showed that the longitude vortex can thicken the otherwise flat surface boundary layer. The typical detailed structure of the longitude vortex caused by the delta winglet on the flat surface boundary layer has been detected by Wu et al. [5]. According to their study, the longitudinal main vortex and the induced vortex can be observed downstream of the winglet. The flow can be divided into two regions, inflow and outflow. They then discovered that an increase in aspect ratio can move the vortex toward to the surface and decrease the turbulent intensity of the flow downstream [6]. The escalation of turbulence fluctuation seems to revert more when the attack angle of the delta winglet increases [7]. The increase of attack angle of the delta winglet can also strengthen the intensity of the swirling motion in a circular tube [8], though it can decrease the vorticity of the longitude vortex for the flat surface case [7].

Oneissi et al. [9] investigated the structure of the turbulence caused by a pair of winglets in a rectangular pipe at different downstream distances. They discussed the vortex

generated by the delta winglet pair and also that of an inclined projected winglet pair. They found that the inclined winglet pair can produce larger vortices in the corner of the rectangular pipe.

It is clear that, due to its fundamental and practical importance, much work has been done on turbulence flow downstream of delta winglets. To our knowledge, however, the effect of the inclination angle of the delta winglet on the resulting vortex over a plane has not been systematically explored. The inclination angle is an important parameter of the winglet which can affect the structure of the vortical flow [9]. This paper aims at understanding the effect of inclination angle on the turbulent flow over a flat plate.

2.2 Nomenclature

B	The uncertainty of bias
c	The chord length of the winglet (mm)
E	The total uncertainty
h	The height of the winglet (mm)
KE	Normalized turbulence kinetic energy
N	Sampling number
P	The uncertainty of precision
Re_h	Reynold number based on the winglet height
TG	Turbulent generator
Tu	Stream-wise turbulence intensity

u_i Instantaneous fluctuating velocity (m/s)

u_{rms} Root-mean-square velocity (m/s)

U_i Instantaneous velocities (m/s)

$\overline{U}$ Time-averaged local velocity (m/s)

U_∞ Time-averaged free-stream velocity (m/s)

v_i Instantaneous fluctuating velocity in Y direction (m/s)

$\overline{V}$ Time-averaged velocity in Y direction (m/s)

w_i Instantaneous fluctuating velocity in Z direction (m/s)

$\overline{W}$ Time-averaged velocity in Z direction (m/s)

α The attack angle of the winglet (degrees)

λ Taylor micro-scale (m)

Λ Integral scale (m)

$\rho(\tau)$ Autocorrelation factor

τ_λ Taylor time scale (s)

τ_Λ Integral time scale (s)

ω The vorticity of the vortex (s^{-1})

Ω Non-dimensional vorticity of the vortex

2.3 Experimentation

The model of the studied winglet is shown in Fig. 2.1. The winglet is made of 0.1mm thick aluminum (1145-H19) sheet. Based on the knowledge gathered from Wu et al. [5], the attack angle α is set at 30 degrees. The height h is 15mm and the chord length c is 30mm, resulting in an aspect ratio *c/h* = 2. The flow was measured by the hotwire with two different inclination angles, $\beta = 90°$ and 120°.

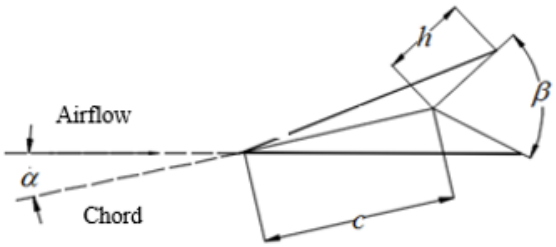

Figure 2. 1. The delta winglet model; c = chord length, h = winglet height, α = attack angle.

The model was placed on the base of the 76cm×76cm cross-section wind tunnel. The winglet was taped in the middle of the test section. The turbulent flow caused by the winglet was measured using a triple sensor hotwire (type 55P95) and a constant-temperature anemometer at 13*h* (200mm) downstream as shown in Fig. 2.2 Flow measurements was acquired over an 100mm×44mm grid with a resolution of 4mm. The free-stream velocity was fixed at 10 m/s, leading to a Reynolds number based on the height of the winglet of 9000 (or 18000 based on the chord length). The instantaneous voltage of three directions were recorded by the hotwire. Then, the instantaneous velocities were deduced from the voltage according to the calibration and the temperature measured by the

probe [10]. The velocity was sampled at 80 kHz and low passed at 30 kHz to avoid aliasing. The sample size was held at 10^6.

(a)

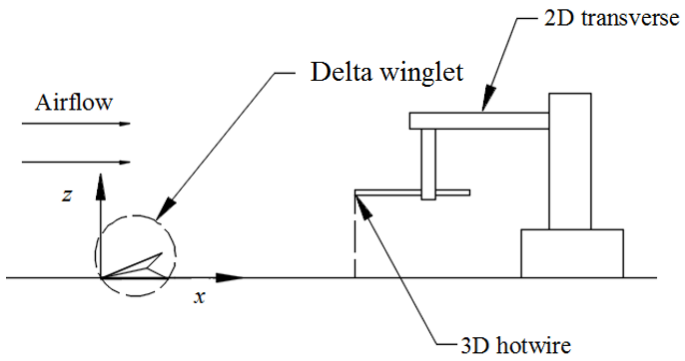

(b)

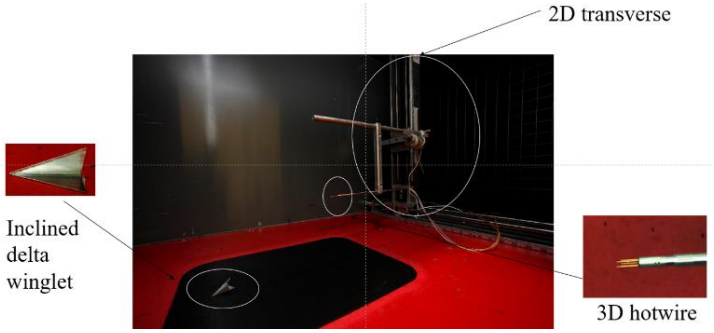

Figure 2. 2 (a) The experiment setup plan, (b) photos detailing the experimental setup.

2.4 Data Analysis

The process of data analysis in Ref [11] was followed. The time-averaged velocity was deduced from:

$$\bar{U} = \frac{1}{N}\sum_{i=1}^{N} U_i \qquad (1)$$

where the sample size was N=10^6. The instantaneous fluctuating velocity (u) was obtained by subtracting the time-averaged velocity from the instantaneous velocity, $u_i = U_i - \bar{U}$. The intensity of this fluctuation was expressed in the root-mean-square form:

$$u_{rms} = \sqrt{\sum_{i=1}^{N} \frac{{u_i}^2}{N-1}} \qquad (2)$$

This turbulence intensity is commonly normalized by the time-averaged free-stream velocity U_∞, i.e.,

$$Tu = \frac{u_{rms}}{U_\infty} \qquad (3)$$

Turbulence is inherently three dimensional [11], and thus, the fluctuation occurs in x, y and z directions. The total turbulent kinetic energy is composed of contributions from the three orthogonal components,

$$KE = \frac{1}{2}\left[\left(\frac{u_i}{U_\infty}\right)^2 + \left(\frac{v_i}{U_\infty}\right)^2 + \left(\frac{w_i}{U_\infty}\right)^2\right] \qquad (4)$$

The integral scale signifies the large, energy containing eddies. It can be calculated from the autocorrelation factor:

$$\rho(\tau) = \frac{\overline{u(t)u(t+\tau)}}{\overline{u^2(t)}} \qquad (5)$$

In the case of discrete data, the auto correlation factor is expressed as:

$$\rho(n\Delta t) = \frac{\frac{1}{N-n}\sum_{i=1}^{N-n}(u_i u_{i+n})}{\frac{1}{N}\sum_{i=1}^{N} u_i^2} \qquad (6)$$

where n varied from 0 to N-1. and the integral time scale is defined as:

$$\tau_\Lambda = \int_0^\infty \rho(\tau)d\tau \qquad (7)$$

For the discrete sample, it is:

$$\tau_\Lambda = \sum_{i=1}^{N_k-1} \rho(i\Delta t)\,\Delta t \qquad (8)$$

where the N_k is the point where the $\rho(\tau)$ first comes to the negative side. The integral scale can be determined, by invoking Taylor frozen hypothesis [11], from:

$$\Lambda = \overline{U}\tau_\Lambda \qquad (9)$$

The Taylor microscale represents the small eddies in the turbulent flow, actively dissipating kinetic energy via viscosity into heat. The Taylor time scale (τ_λ) can be [12] expressed as:

$$\tau_\lambda = \sqrt{\frac{\overline{2u_\iota{}^2}}{(\frac{du_i}{dt})^2}} \qquad (10)$$

When the data is discrete,

$$\tau_\lambda = \sqrt{\frac{\frac{1}{N}\sum_{i=1}^{N} 2u_i^2}{\frac{1}{N-1}\sum_{i=1}^{N-1}(\frac{u_{i+1}-u_i}{\Delta t})^2}} \qquad (11)$$

According to the Taylor frozen hypothesis [12], eddies may be considered to be merely passing through the probe without evolution if the velocity fluctuation is small compared to the convective current that carries the eddies. Therefore, the Taylor micro-scale can be obtained from:

$$\lambda = \bar{U}\tau_\lambda \qquad (12)$$

The vorticity of the longitude vortex can be defined as:

$$\omega = \frac{\partial \bar{W}}{\partial y} - \frac{\partial \bar{V}}{\partial z} \qquad (13)$$

An appropriate non-dimensional vorticity can be formed by multiplying ω by the height of the delta winglet, h, and dividing by the time-averaged free-stream velocity U_∞, i.e.,

$$\Omega = \frac{\omega \times h}{U_\infty} \qquad (14)$$

The total uncertainty (E) of each flow parameter consists of bias uncertainty (B) arising from the process of calibrating of the hotwire, and the precision (P) uncertainty due to random variations when repeating the acquisition of the instantaneous velocity data. The process in Ref [13] was followed; see the Appendix.

2.5 Results and Discussion

To elucidate the effect of the inclination angle of the delta winglet on the flow downstream, the large longitude vortex was first captured and analyzed. Cross-sectional velocity vector plots complemented with stream-wise velocity contours work well. The turbulence in the flow field was delineated in terms of the turbulent intensity, the integral length and Taylor microscale.

2.5.1 Vortex Structure

The cross-stream (*Y*-*Z* plane) velocity vectors and the stream-wise velocity contours are depicted in Fig. 2.3; where *Y*/*h* = 0 (*X*/*h* = 0, *Z*/*h* = 0) corresponds to the leading edge of the delta winglet. The studied area, as shown in the figure, was at 13*h* (200mm) downstream from the leading edge of the delta winglet. The contours of the stream-wise

time-averaged velocity normalized by U_∞ ($\approx$ 10 m/s) portray the winglet perturbed boundary layer flow behavior. The dotted triangle profile depicts the winglet upstream. The uncertainty of the mean velocity in this study is approximately 0.28 m/s; see Appendix A.

The generation of the longitude vortex had been speculated to initiate from the leading edge of the delta winglet [6, 14]. The generated vortex had been found to persist far downstream [15, 16]. Comparing the vortex caused by an inclined winglet, the induced flow could be divided into two regions. The region where the cross-stream velocity vectors (in the *Y*-*Z* plane) point toward the surface is the **inflow region**; see Fig. 2.3(b). For a heated surface, the vortex would bring the cooler freestream air down, toward the hot surface in this region. And the region where the flow moves upward, away from the surface is called the **outflow region**; see Fig. 2.3(b). It is clear from Fig. 2.3 that the prevailing vortex rotates anticlockwise looking upstream. In agreement with previous studies [6, 17], the outflow region corresponds to the right (looking upstream onto the winglet) of the tailing edge. The inflow region has a larger stream-wise velocity, as the inner boundary layer is pushed toward the plate, than the outflow region.

(a)

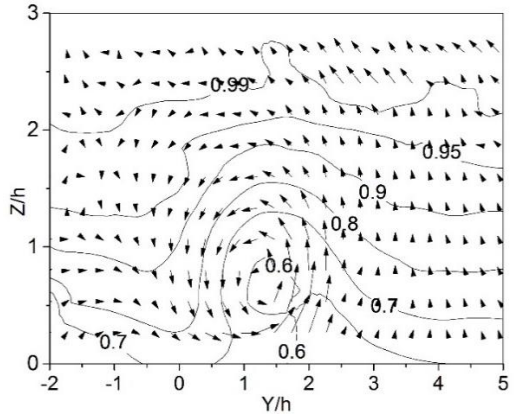

(b)

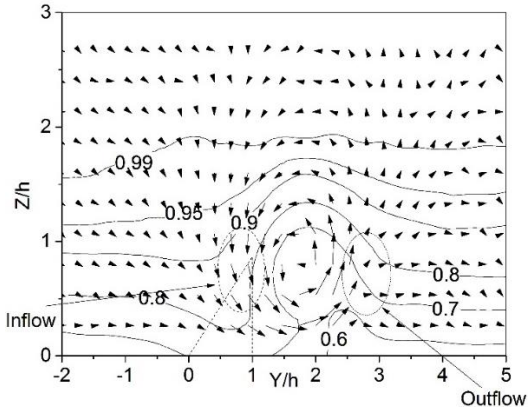

(c)

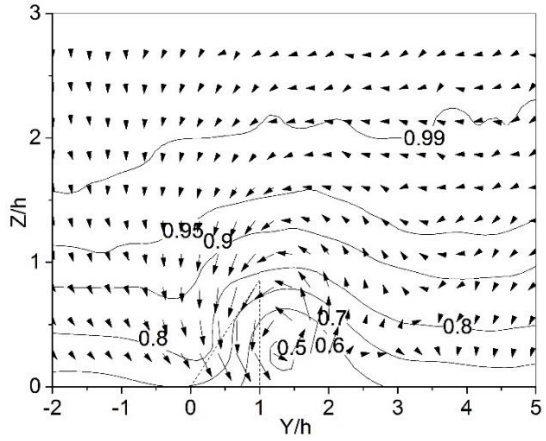

Figure 2. 3 Velocity vectors in the YZ plane and stream-wise time-averaged velocity contours normalized by U_∞ at (a) 13h (200mm) downstream with $\beta =$

90°, (b) 13h (200mm) downstream with $\beta = 120°$, (c) 6.7h (100mm) downstream with $\beta = 120°$.

In other words, the longitude vortex has a significant effect on the thickness of the turbulent boundary layer. In the current setup, the thickness of the boundary layer without the delta winglet was around 1.6h (24 mm). The swirling motions generated by the vortex generator is known to disrupt the boundary layer and create significant mixing downstream [18, 19]. Consequently, the boundary layer in the current study thickened to slightly more than 2h for the $\beta = 90°$ case, and to slightly less than 2h at a larger inclination angle, $\beta = 120°$. The inner boundary layer (< 0.95 freestream stream-wise velocity) thickness (contour or profile) was skewed by the toward-the-plate in the inflow region and that out-of-the-plate in the outflow region. The more symmetrical stream-wise velocity contours along with the less-thickened boundary layer for the larger inclination angle ($\beta = 120°$) case seems to suggest a lesser flow agitation, compared to the $\beta = 90°$ case. Also, the boundary layer is less skewed at 100 mm, where the corresponding vortex is smaller. This implies that the vortex-boundary layer interactions evolve with distance downstream.

To further elucidate the flow field, especially the inflow and outflow regions, the average of normalized $\overline{W}$ velocities are depicted in Fig. 2.4. The location of the lowest and the largest average $\overline{W}/U_\infty$ along the studied Y span correspond nicely to the locations of inflow and outflow. The vortex shifts to the right (looking upstream) by about 0.5h (8mm) as the inclination angle increases from 90° to 120°. This is because the cross section of the winglet moves to the right (looking upstream) and thus the flow is deflected to the right

(outflow side) as β increases. The larger inclination also resulted in a more negative $\overline{W}/U_\infty$ in the inflow region and a less positive $\overline{W}/U_\infty$ in the outflow region. The entire vortex structure shifts about 4 mm to the outflow side, with increasing distance from 100 to 200 mm. Furthermore, the vortex expands as it evolves downstream.

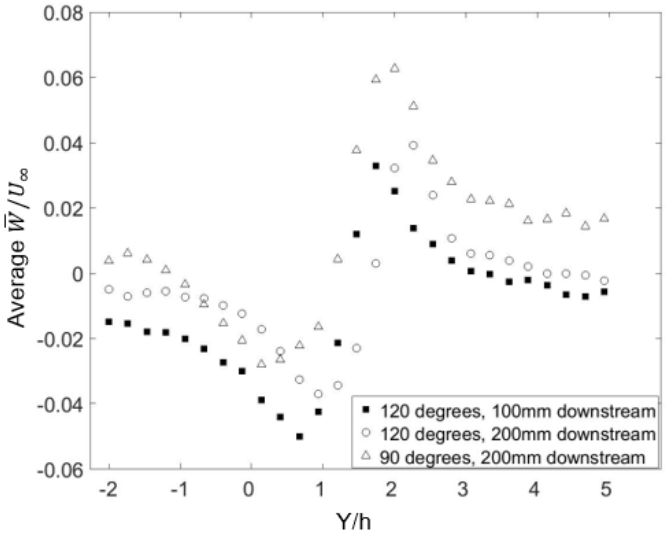

Figure 2. 4 Average of $\overline{W}/U_\infty$ in the Y direction.

The normalized stream-wise velocity profile at the location of the prevailing vortex center is shown in Fig. 2.5. The peak stream-wise velocity deficit can be observed around the center of the longitude vortex, which agrees with Godarad and Stanislas [20]. Increasing the inclination angle from 90° to 120° appears to lead to smaller maximum stream-wise velocity deficits. The stream-wise peak deficit is much larger at the shorter downstream distance of 100 mm.

To better identify the longitude vortex in the *YZ* plane, the vorticity is depicted in Fig. 2.6. A high vorticity region can be found at the core of the vortex, concurring with Luo et al. [21]. The vorticity of the vortex core decreases as the vortex travels downstream. The location of the vortex core moves upward as the inclination angle increases (*Z/h*=0.53 for $\beta = 90°$ and 0.8 for $\beta = 120°$). It also shifts farther downstream. The winglet-generated vortex expands as it travels downstream, i.e., the vortex at 100 mm is smaller than that at 200 mm, see Fig. 2.4. The height of the vortex core corresponds to the location of the peak deficit of the stream-wise velocity shown in Fig. 2.5. With the increase of inclination angle, the prevailing longitude vortex shrinks according to the contour of the vorticity. The main vortex separates from the bottom wall in the outflow region. Moreover, a smaller vortex rotating opposite to the main vortex can be observed at the outflow region side. It is called induced vortex according to Biswas et al. [22]. Only one induced vortex can be observed, presumably because the measurement location is quite far downstream, where smaller (induced) vortices may have decayed [23].

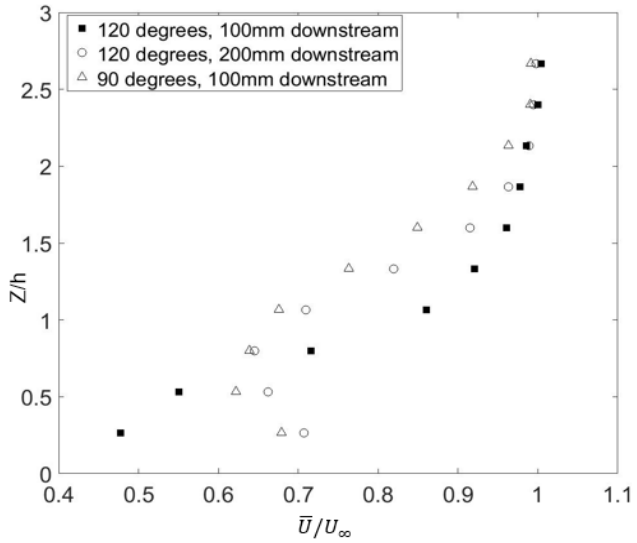

Figure 2. 5 Stream-wise velocity normalized by the freestream velocity in the center of the vortex (Y/h=1.2, when $\beta = 90°$, 200mm downstream; Y/h = 1.7, when $\beta = 120°$, 200mm downstream; Y/h = 1.4, when $\beta = 120°$, 100mm downstream).

(a)

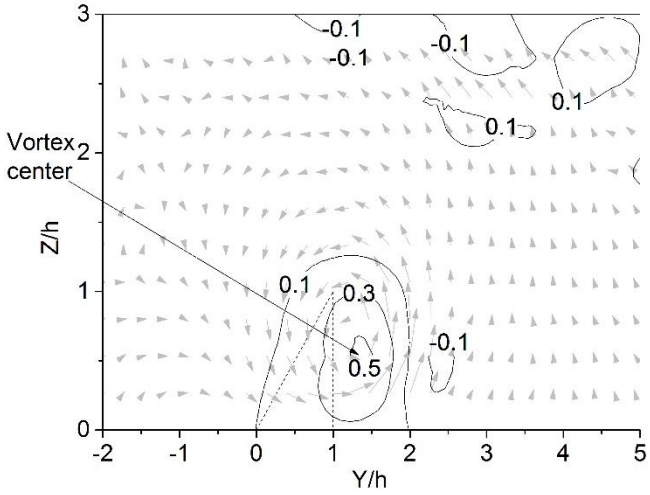

(b)

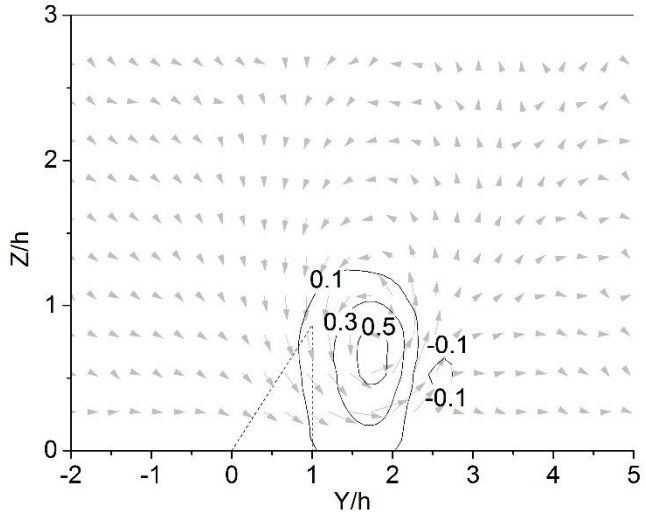

(c)

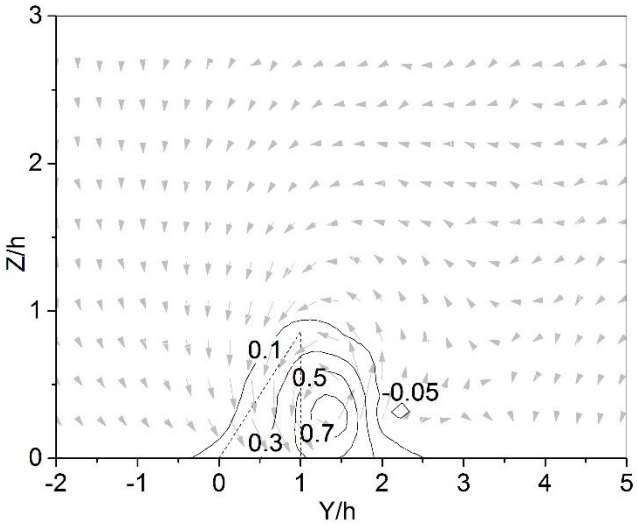

Figure 2. 6 Cross-stream vorticity contours at (a) 13h (200mm) downstream, $\beta = 90°$, (b) 13h (200mm) downstream, $\beta = 120°$, (c) 6.7h (100mm) downstream, $\beta = 120°$

2.5.2 Turbulent intensity

Turbulent intensity in the flow is the key parameter to quantify the turbulence. Fig. 2.7 shows the stream-wise turbulence intensity (*Tu* is the local turbulence root-mean-square fluctuation, u_{rms}, normalized by the freestream time-averaged velocity, U_∞), contours at 13*h* (200 mm) downstream of the winglet. The *Tu* value decreases with increasing inclination angle, and this coincides with the shrinking of the main vortex shown in Fig. 2.6. The peak stream-wise turbulence intensity (*Tu*≈0.09) is above the core of the vortex, at *Z*/*h*≈1.4. As expected, this corresponds to the location of highest shear stress (velocity gradient); see Fig. 2.5. With vortex shrinkage, the peak turbulent intensity region is smaller, and it moves closer to the surface, when $\beta = 120°$. *Tu* decreases from the proximity of the solid surface to the freestream in both of the inflow and the outflow region, confirming the low background turbulence outside the perturbed boundary layer, i.e., in the freestream. More importantly, *Tu* is larger in the inflow region, compared to that in the outflow region. This is presumably due to the larger flow (stream-wise velocity as depicted in Fig. 2.3) and shear. The average turbulent intensity when $\beta = 90°$ is 12% higher than that at a higher inclination angle of $\beta = 120°$. The uncertainty of the normalized freestream turbulent intensity is around 0.004.

(a)

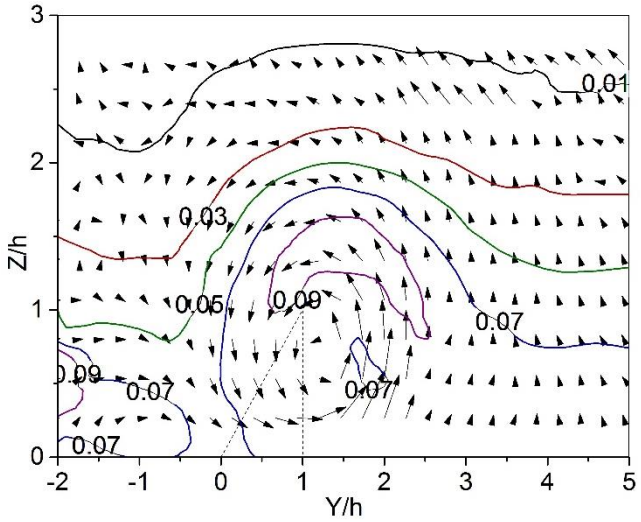

(b)

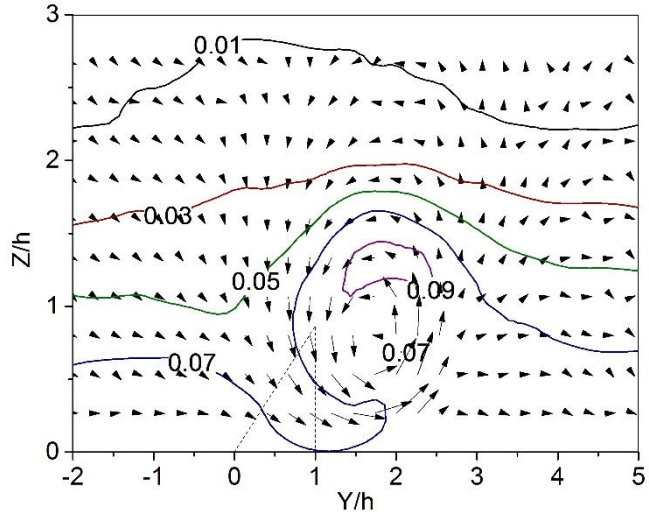

Figure 2. 7 Turbulent intensity in the stream-wise direction (Tu) and velocity vectors in the YZ plane at 13h (200mm) downstream (a) $\beta = 90°$, (b) $\beta = 120°$.

Downstream of a winglet, the turbulent intensity of the stream-wise velocity can be quite different from those in the *Y* and *Z* directions [5]. Some of the energy generated from

the stream-wise flow is converted to the rotating motion of the vortex, and the rest is transformed into turbulent kinetic energy. To have a better understanding of the turbulent kinetic energy budget, the stream-wise *KE* is plotted in Fig. 2.8.

(a)

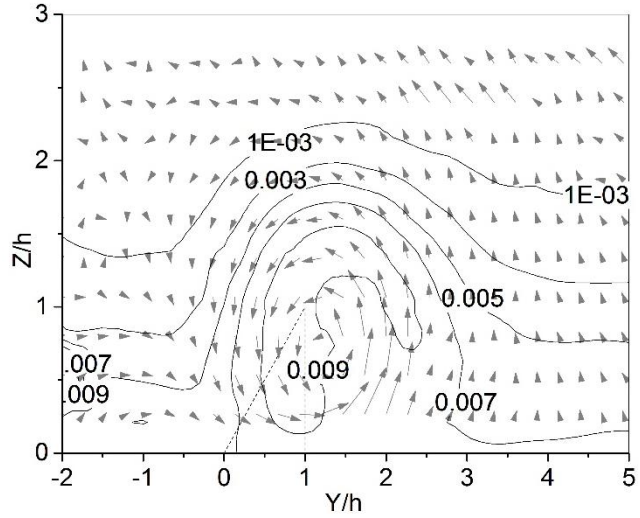

(b)

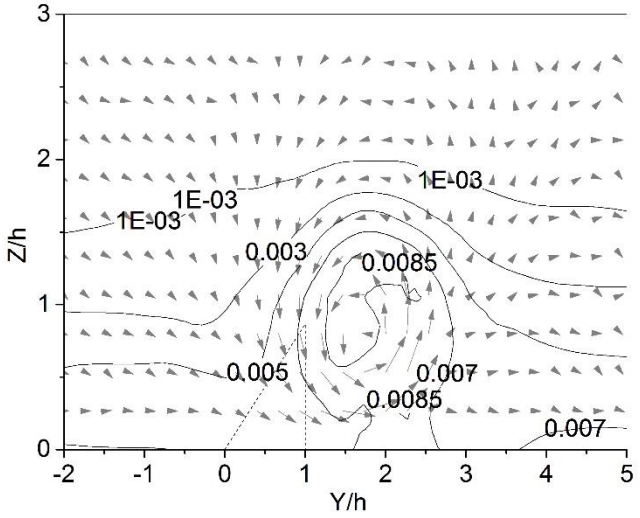

Figure 2. 8 Normalized stream-wise turbulent kinetic energy and velocity vectors in the YZ plane at 13h (200mm) downstream (a) $\beta = 90°$, (b) $\beta = 120°$.

The contours of the turbulent kinetic energy in Fig. 2.8 follow the shape of the vortex. It can be observed that the region near the core of the longitude vortex generates the largest energy from the flow to turbulence. The peak deficit of stream-wise velocity in the core of the vortex also confirms that. Inflow and outflow regions are the high turbulent kinetic energy regions when the delta winglet is used in the circular pipe [15]. The stream-wise turbulence kinetic energy decreases as the distance from the core increases. And the delta winglet generates less turbulent kinetic energy from the flow as the inclination angle increases, which conforms to the decrease of deficit in the stream-wise velocity (see Fig. 5).

2.5.3 Integral Scale

Integral scale signifies the energy containing eddies. Contours of stream-wise integral scale, where the associated uncertainty is roughly 6mm, are portrayed in Fig. 2.9. The integral scale is undefined outside the perturbed boundary layer, where the flow is largely non-turbulent. Hence, only the integral around the vortex is shown in Fig. 2.9.

(a)

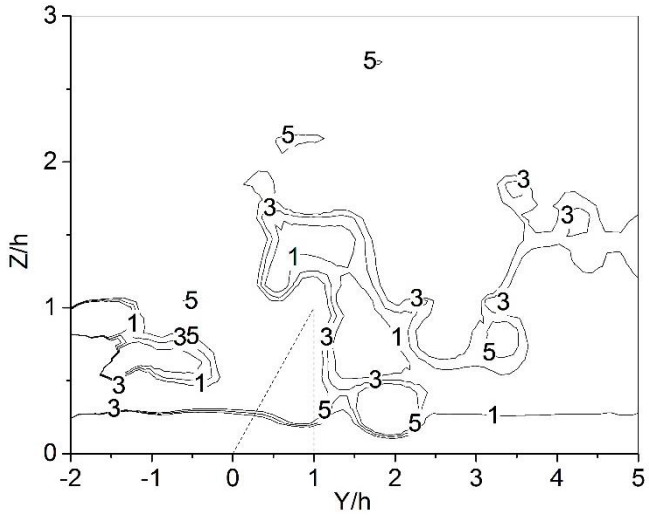

(b)

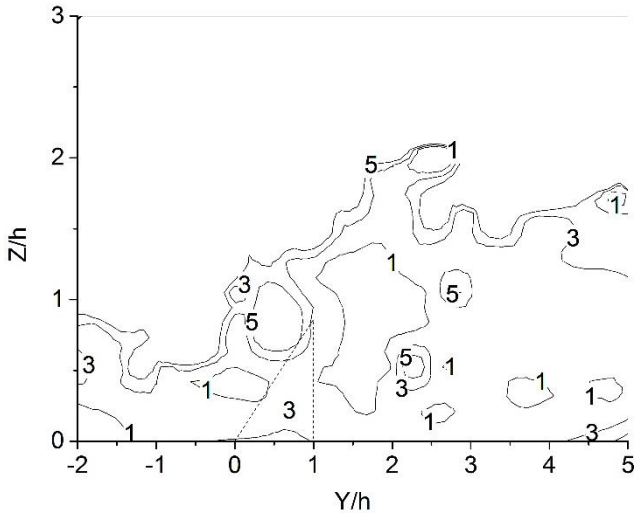

Figure 2. 9 Stream-wise integral scale normalized by h contours at 13h (200 mm) downstream (a) $\beta = 90°$, (b) $\beta = 120°$.

The stream-wise integral scale around the longitudinal vortex appears to be consistently larger; correlate Fig. 2.9 with Fig. 2.6. Even though what is plotted is the stream-wise integral scale, and thus, it is more-or-less perpendicular to the longitudinal vortex, its contours, nonetheless, still indicate the longitudinal vortex, which is primarily in the *YZ* plane. Specifically, the smallest stream-wise integral scale inside the 1h contour matches reasonably well with the vortex core shown in Fig. 2.6. When comparing the average integral scale, the larger inclination angle, $\beta = 120°$, produced integral scale which is 21% smaller than that generated by $\beta = 90°$.

2.5.4 Taylor Microscale

Taylor microscale represents the small and dissipative eddies in the flow [10]. The overall contour view of stream-wise Taylor microscale is shown in Fig. 2.10. The uncertainty of the Taylor microscale is estimated to be around 0.6mm; see Appendix.

(a)

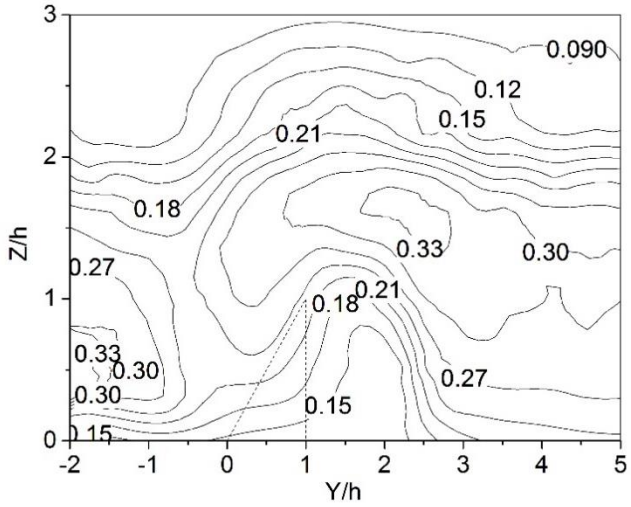

(b)

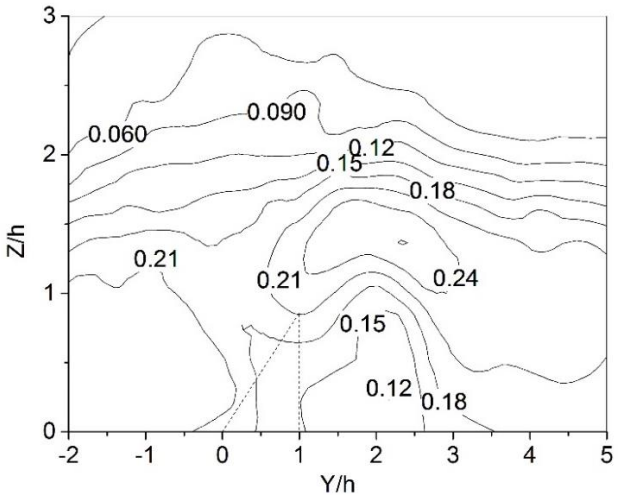

Figure 2. 10 Contours of stream-wise Taylor microscale normalized by h at 13h (200 mm) downstream (a) $\beta = 90°$, (b) $\beta = 120°$.

The Taylor microscale peaked around *Y/h*≈2.5 and *Z/h*≈1.5, and *Y/h*≈2 and *Z/h*≈1.3, for $\beta = 90°$ and 120°, respectively. These roughly coincide with the maximum stream-wise turbulent intensity zones in Fig. 2.7. Within the longitudinal vortex region, the smallest Taylor microscale is detected next to the solid surface bounded by the inflow and outflow. It appears that the inflow might have some compression effect, resulting in the occurrence of the smallest Taylor microscale within the disturbed boundary layer. Outside the boundary layer, where the background turbulence is low, the notion of Taylor microscale is questionable. That is, the Taylor microscale contours far from the solid surface (> *Z/h*=2) should be disregarded. The larger inclination angle which produced a weaker longitudinal vortex also resulted in smaller Taylor microscale, approximately 26%

smaller. This appears to suggest more restrained (to near solid surface) and hence, smaller λ, and weaker vortical flow for the $\beta = 120°$ case.

2.6 Conclusion

The role of the inclination angle $\beta = 90° \& 120°$ of a *c/h* = 2 (*c* = winglet chord length, h = winglet height) delta winglet at 30° with respect to an Re_h = 9000 wind was experimentally investigated. The evolution of the vortical flow was quantified in terms of vortex size, vorticity, turbulence intensity, integral length and Taylor microscale. The boundary layer is found to be progressively disturbed as the vortical flow-boundary layer interactions evolve. The longitude vortex enlarges and shifts to the outflow side as it travels downstream. With the increase of inclination angle, the longitudinal vortex is reduced and shifted toward the outflow side. Along with the shrinking of the longitudinal vortex is a reduced turbulent boundary layer. Moreover, the into-the-plate velocity in the inflow region increases, but the corresponding out-of-plate velocity in the outflow region decreases, with increasing inclination angle. The perturbed flow field turbulence, along with the associated integral scale and Taylor microscale, are also lowered when increasing β from 90° to 120°.

Acknowledgement

This work was made possible by Natural Sciences and Engineering Research Council of Canada and Ontario Centres of Excellence.

References

[1] R. L. Webb and N. Kim, "Enhanced Heat Transfer," Taylor and Francis, New York, 1994.

[2] A. Boonloi and W. Jedsadaratanachai, "Flow topology, heat transfer characteristic and thermal performance in a circular tube heat exchanger inserted with punched delta winglet vortex generators," J. Mech. Sci. Technol., vol. 30, no. 1, pp. 457–471, 2016.

[3] L. Luo, F. Wen, L. Wang, B. Sundén, and S. Wang, "Thermal enhancement by using grooves and ribs combined with delta-winglet vortex generator in a solar receiver heat exchanger," Appl. Energy, vol. 183, pp. 1317–1332, 2016.

[4] P. Eibeck and J. Eaton, "Heat transfer effects of a longitudinal vortex embedded in a turbulent boundary layer," ASME. J. Heat Transf., vol. 109, no. 1, pp. 16–24, 1987.

[5] H. Wu, D. S-K. Ting, and S. Ray, "An experimental study of turbulent flow behind a delta winglet," Exp. Therm. Fluid Sci., vol. 88, pp. 46-54, 2017.

[6] H. Wu, D. S-K. Ting, and S. Ray, "Flow over a flat surface behind delta winglet of varying aspect ratio," Int. J. Heat Mass Transf., vol. 120, pp. 117–126, 2017.

[7] H. Wu, D. S.-K. Ting, and S. Ray, "The effect of delta winglet attack angle on the heat transfer performance of a flat surface," Int. J. Heat Mass Transf., vol. 120, pp. 117–126, 2018.

[8] Y. Lei, F. Zheng, C. Song, and Y. Lyu, “Improving the thermal hydraulic performance of a circular tube by using punched delta-winglet vortex generators,” Int. J. Heat Mass Transf., vol. 111, pp. 299–311, 2017.

[9] M. Oneissi, C. Habchi, S. Russeil, D. Bougeard, and T. Lemenand, “Novel design of delta winglet pair vortex generator for heat transfer enhancement,” Int. J. Therm. Sci., vol. 109, pp. 1–9, 2016.

[10] F.E. Jørgensen, “How to Measure Turbulence with Hot-Wire Anemometers: A Practical Guide, Dantec Dynamics, Skovlunde,” Denmark, 2002.

[11] D. S-K. Ting, “Basics of Engineering Turbulence,” Academic Press, New York, 2016.

[12] G. I. Taylor, “The spectrum of turbulence,” Proc. R. Soc. Lond. Ser. Math. Phys. Sci., pp. 476–490, 1938.

[13] R. S. Figliola and D. E. Beasley, “Theory and Design for Mechanical Measurements”, IOP Publishing, 2001.

[14] L. Li, X. Du, Y. Zhang, L. Yang, and Y. Yang, “Numerical simulation on flow and heat transfer of fin-and-tube heat exchanger with longitudinal vortex generators,” Int. J. Therm. Sci., vol. 92, pp. 85–96, 2015.

[15] Y. Xu, M. Islam, and N. Kharoua, “Experimental study of thermal performance and flow behaviour with winglet vortex generators in a circular tube,” Appl. Therm. Eng., vol. 135, pp. 257–268, 2018.

[16] Y. Xu, M. Islam, and N. Kharoua, “Numerical study of winglets vortex generator effects on thermal performance in a circular pipe,” Int. J. Therm. Sci., vol. 112, pp. 304–317, 2017.

[17] A. Jacobi and R. Shah, “Heat transfer surface enhancement through the use of longitudinal vortices: a review of recent progress,” Exp. Therm. Fluid Sci., vol. 11, no. 3, pp. 295–309, 1995.

[18] P. Saha, G. Biswas, and S. Sarkar, “Comparison of winglet-type vortex generators periodically deployed in a plate-fin heat exchanger–A synergy based analysis,” Int. J. Heat Mass Transf., vol. 74, pp. 292–305, 2014.

[19] L. Tang, W. Chu, N. Ahmed, and M. Zeng, “A new configuration of winglet longitudinal vortex generator to enhance heat transfer in a rectangular channel,” Appl. Therm. Eng., vol. 104, pp. 74–84, 2016.

[20] G. Godard and M. Stanislas, “Control of a decelerating boundary layer. Part 1: Optimization of passive vortex generators,” Aerosp. Sci. Technol., vol. 10, no. 3, pp. 181–191, 2006.

[21] L. Luo, F. Wen, L. Wang, B. Sunden, and S. Wang, “On the solar receiver thermal enhancement by using the dimple combined with delta winglet vortex generator,” Appl. Therm. Eng., vol. 111, pp. 586–598, 2017.

[22] G. Biswas, K. Torii, D. Fujii, K. Nishino, “Numerical and experimental determination of flow structure and heat transfer effects of longitudinal vortices in a channel flow,” Int. J. Heat Mass Transf., vol. 39, pp. 3441–3451, 1996.

[23] C. M. Velte, M. O. Hansen, and V. L. Okulov, “Multiple vortex structures in the wake of a rectangular winglet in ground effect,” Exp. Therm. Fluid Sci., vol. 72, pp. 31–39, 2016.

[24] S. Yavuzkurt, “A guide to uncertainty analysis of hot-wire data,” J. Fluids Eng., vol. 106, no. 2, pp. 181–186, 1984.

CHAPTER 3

THE ROLE OF DELTA WINGLET INCLINATION ANGLE ON HEAT TRANSFER ENHANCEMENT

3.1 Introduction

Many kinds of turbulent generators (TG) have been applied to enhance heat transfer via the resulting flow turbulence and vorticity [1,2]. Among them, delta winglet (DW) is a promising enhancer as it can generate a longitudinal vortex street in addition to promoting flow turbulence. The vortex street tends to survive far downstream, resulting in a prolonged area with augmented heat transfer rate [3,4]. Among the delta winglet heat transfer enhancement studies are those that focus on heat exchangers [5-7], circular tubes [8, 9], heated plates and channels [10, 11]. Pal et al. [5] numerically investigated a pair of delta winglets upstream of two tubes in a heat exchange channel. Over their studied conditions, the average heat transfer rate was augmented by about 40%. Liang et al. [8] numerically studied heat transfer behavior in a circular pipe fitted with arrays of delta winglets. They correlated the surface Nusselt number contours with the flow mixing effect. Syaiful et al. [10] examined the flow over a heated plate mounted with delta winglet pairs. They showed that perforating the winglet with some holes can decrease the pressure drop without significantly losing the efficacy of heat transfer augmentation.

From the literature, it is evident that attack angle, aspect ratio and inclination angle are key parameters affecting winglet-enhanced heat transfer. Wu et al. [12] varied the attack angle of their delta winglet from 30 to 60°, and found that, within the considered conditions, the attack angle of 60° gave the most significant heat transfer enhancement in

the near wake region of a heated flat surface. In Lei et al. [13] heat exchanger study, it is shown that the thermal performance improved when increasing the aspect ratio from 1 to 2, beyond which the enhancement decreases. Oneissi et al. [14] examined the effect of the inclination angle of a winglet pair inside a rectangular pipe. They discovered that the inclined winglet pair which produced large secondary flow in the corner of the rectangular pipe gave the best heat transfer performance.

It is clear that much work has been performed on the thermal performance of a delta winglet due to its efficiency, economy, manufacturing simplicity and maintenance ease. Moreover, a modest change in one of the key winglet parameters can significantly change the resulting heat transfer rate. Among the influential delta winglet parameters, inclination angle seems to be least studied, especially regarding its effect on the heat transfer rate from an unconfined flat surface. Unconfined surface heat transfer is applicable in cooling of a solar panel [12] or the flat side of a permanent magnet synchronous generator coil [15], among many other applications. As such, this paper aims at improving our understanding of the effect of delta winglet inclination angle on the thermal performance of a flat plate.

3.2 Nomenclature

AR	Aspect ratio
c	The chord length of the winglet (mm)
D	Characteristic length (m)
DW	Delta winglet
h	The height of the winglet (mm)

$h_{convection}$	The local convection heat transfer coefficient (W/(m2·K))
$h_{convection,\ 0}$	The local convection heat transfer coefficient without delta winglet (W/(m^2·K))
k_{air}	The conductivity of air (W/(m·K))
k_{PTFE}	Conductivity of the PTFE plate (W/(m·K))
K	Normalized turbulence kinetic energy
$\overline{K}$	Averaged turbulent kinetic energy
Nu	Local Nusselt number
Nu_0	Local Nusselt number without delta winglet
PTFE	Polytetrafluoroethylene
$Q_{convection}$	Heat convected away to the freestream (W)
$Q_{radiation}$	Heat radiated to the air (W)
Q_{tot}	Total heat conducted to the upper surface (W)
Re_h	Reynold number based on the winglet height
t_{PTFE}	Thickness of PTFE plate (mm)
T_{bottom}	Temperature at the bottom surface of PTFE plate (100℃)
TG	Turbulent generator

$T_{surrounding}$	Surrounding temperature (22℃)
T_{top}	Temperature at the upper surface of PTFE plate (℃)
u_i	Instantaneous fluctuating velocity (m/s)
u_{rms}	Root-mean-square velocity (m/s)
U_i	Instantaneous velocities (m/s)
$\overline{U}$	Time-averaged local velocity (m/s)
U_∞	Time-averaged free-stream velocity (m/s)
v_i	Instantaneous fluctuating velocity in Y direction (m/s)
$\overline{V}$	Time-averaged velocity in Y direction (m/s)
w_i	Instantaneous fluctuating velocity in Z direction (m/s)
$\overline{W}$	Time-averaged velocity in Z direction (m/s)
α	The attack angle of the winglet (degrees)
σ	Boltzmann's constant (5.67×10^{-8} Wm^{-2} K^{-4})
ω	The vorticity of the vortex (s^{-1})
Ω	Non-dimensional vorticity of the vortex

3.3 Experimentation

The studied winglet model is shown in Fig. 3.1. It is made of 0.1 mm thick aluminum (1145-H19) sheet. Based on the knowledge gathered from Wu et al. [12] and He et al. [16], the attack angle, α, is set at 30 degrees. The height of the delta winglet, h, is 15mm and the chord length, c, is 30 mm, leading to an aspect ratio c/h = 2. Three different inclination angles, 60°, 90° and 120°, were considered at a free-stream velocity of 7 m/s, i.e., a Reynolds number based on the height of the winglet, Re_h, of 6300.

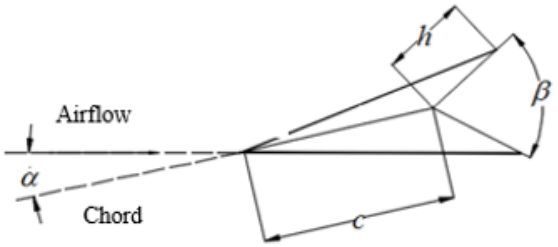

Figure 3. 1 The delta winglet model; chord length, c = 30 mm, winglet height, h = 15 mm, attack angle, α = 30 degrees, inclination angle, β = 60°, 90°, 120°.

The model was placed in a 76cm×76cm cross-section wind tunnel over a 3 mm thick, 295 mm wide and 380 mm long PTFE (Polytetrafluoroethylene) plate. The conductivity of the PTFE plate was 0.25 W/(m·K), while its emissivity was 0.92. The winglet was taped onto the plate as shown in Fig. 3.2. A heated water tank was placed underneath to generate steam which maintained the bottom surface of the PTFE plate at 100℃. The convective heat transfer enhancement was deduced based on the temperature on the top surface measured by Flir C2 thermal camera calibrated by a K type thermocouple

with an accuracy of 0.5°C. A thermal camera with a resolution of 60×80 pixels was positioned 0.5 m above the heated plate.

The delta-winglet-generated turbulent flow over the unheated PTFE plate was characterized with the help of a triple sensor hotwire (type 55P95) and a constant-temperature anemometer. As the augmentation of the heat transfer rate over a reasonable stretch of the plate is of interest, the developed velocity field of a typical cross-section at 13*h* (200mm) downstream from the leading edge of the winglet was scrutinized. Following the procedure detailed in Ref [17], instantaneous velocities were deducted from the measured voltages over a $90\text{mm} \times 40\text{mm}$ grid with a resolution of 4mm. To ensure reliability, a total of 10^6 data points per hotwire were sampled at 80 kHz, and low passed at 30 kHz to avoid aliasing.

(a)

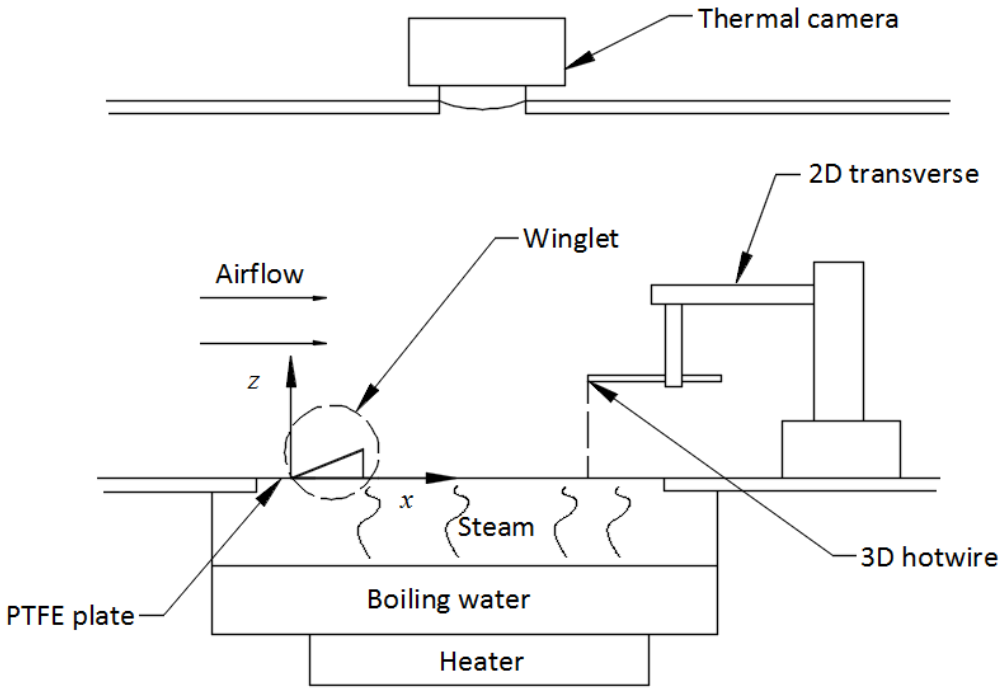

(b)

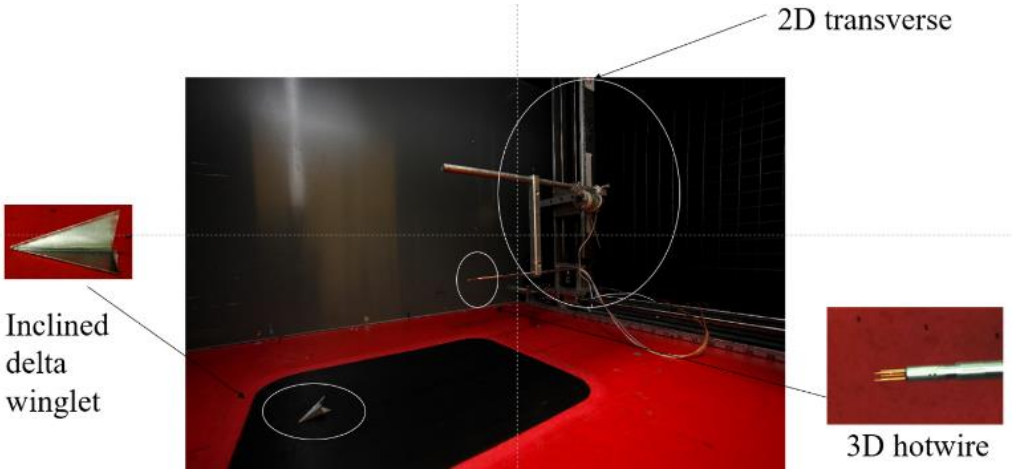

Figure 3. 2 The experiment setup

3.4 Data Analysis

The total heat conducted through the PTFE plate,

$$Q_{tot} = \frac{k_{PTFE} A (T_{bottom} - T_{top})}{t_{PTFE}} \quad (1)$$

where PTFE plate conductivity, k_{PTFE}, was 0.25 W/(m·K), the local heat transfer area, A, was one pixel on the thermal photo (approximately 20 mm^2), the thickness of the PTFE plate, t_{PTFE}, was 3mm, the temperature of the bottom surface, T_{bottom}, was 100℃, and the top surface temperature, T_{top}, was measured by the thermal camera. The heat conducted to the top surface was assumed to be either radiated or convected away by the freestream. The rate of heat radiated to the surrounding can be deduced from:

$$\dot{Q}_{radiation} = \sigma A(T_{top}^4 - T_{surrounding}^4) \quad (2)$$

the Boltzmann's constant, σ, was $5.67 \times 10^{-8} Wm^{-2}K^{-4}$, and the surrounding temperature, $T_{surrounding}$, was approximately 295 K. The convection heat transfer rate was thus obtained from the total heat transfer rate minus that radiated to the surrounding, i.e.,

$$Q_{convection} = Q_{tot} - Q_{radiation} \quad (3)$$

The convection heat transfer coefficient is defined as:

$$\mathrm{h}_{convection} = \frac{Q_{convection}}{A(T_{top} - T_{surrounding})} \quad (4)$$

So, the corresponding non-dimensional Nusselt number is:

$$\mathrm{Nu} = \frac{\mathrm{h}_{convection} D}{k_{air}} \quad (5)$$

Here, D is the characteristic length and $\mathrm{k_{air}}$ is the conductivity of the air. To evaluate the enhancement of the heat transfer, the measured Nusselt number in the presence of the delta winglet was normalized by the corresponding local Nusselt number without the winglet, i.e.,

$$\frac{\mathrm{Nu}}{\mathrm{Nu_0}} = \frac{\mathrm{h}_{convection}}{\mathrm{h}_{convection,0}} \quad (6)$$

The time-averaged velocity was deduced from [17]:

$$\bar{U} = \frac{1}{N}\sum_{i=1}^{N} U_i \tag{7}$$

where the sample size is N=10^6. The instantaneous fluctuating velocity (u) was obtained by subtracting the time-averaged velocity from the instantaneous velocity, $u_i = U_i - \bar{U}$. The intensity of this fluctuation was expressed in root-mean-square form:

$$u_{rms} = \sqrt{\sum_{i=1}^{N} \frac{{u_i}^2}{N-1}} \tag{8}$$

Turbulence is inherently three dimensional [18], and thus, the fluctuations occur in x, y and z directions. The total turbulent kinetic energy is composed of contributions from the three orthogonal components,

$$K = \frac{1}{2}\left[\left(\frac{u_{rms}}{U_\infty}\right)^2 + \left(\frac{v_{rms}}{U_\infty}\right)^2 + \left(\frac{w_{rms}}{U_\infty}\right)^2\right] \tag{9}$$

The vorticity of the longitude vortex can be defined as:

$$\omega = \frac{\partial \bar{W}}{\partial y} - \frac{\partial \bar{V}}{\partial z} \tag{10}$$

Appropriate non-dimensional vorticity can be formed by multiplying ω by the height of the delta winglet, h, and dividing it by the time-averaged free-stream velocity, U_∞, i.e.,

$$\Omega = \frac{\omega \times h}{U_\infty} \tag{11}$$

The total uncertainty (E) of each measurement consists of bias uncertainty (B) and precision uncertainty (P). The bias uncertainty came from the calibration process. The precision (P) uncertainty was due to the random variations when repeating the acquisition of the data; instantaneous velocity data by using the hotwire and the temperature data via the thermal camera. The procedure in Ref [19] was followed when estimating the pertinent uncertainties; see the Appendix A.

3.5 Results and Discussion

The temperature distribution along the PTFE plate was captured and analyzed to reveal the effect of the inclination angle of the winglet on the thermal performance. The results are presented in terms of the Nusselt number normalized by the reference Nusselt number without the delta winglet. Detailed flow measurements obtained in the developed vortical flow region at 13h downstream of the winglet were used to explain the heat transfer behavior.

3.5.1 Heat Transfer

To evaluate the convective heat transfer enhancement caused by the delta winglet, the temperature of the upper surface of PTFE plate was captured by a thermal camera. The local normalized Nusselt numbers were used to illustrate the thermal performance of the turbulent flow. Figure 3.3 depicts the normalized Nusselt number contours. Point (0,0) corresponds to the location of the leading edge of delta winglet; see Fig. 3.2. The triangular island at X/h ≤ 2 is the delta winglet, where high-conductivity aluminum ‘fin’ drastically

augmented the local heat transfer rate. The cross-sectional span in the Y direction of the notably enhanced heat transfer area increases with distance downstream up to X/h around 12 or so. This is presumably due to the expansion of longitude vortex as it evolves downstream [20]. The uncertainty of normalized Nusselt number is approximately 0.06, see Appendix A.

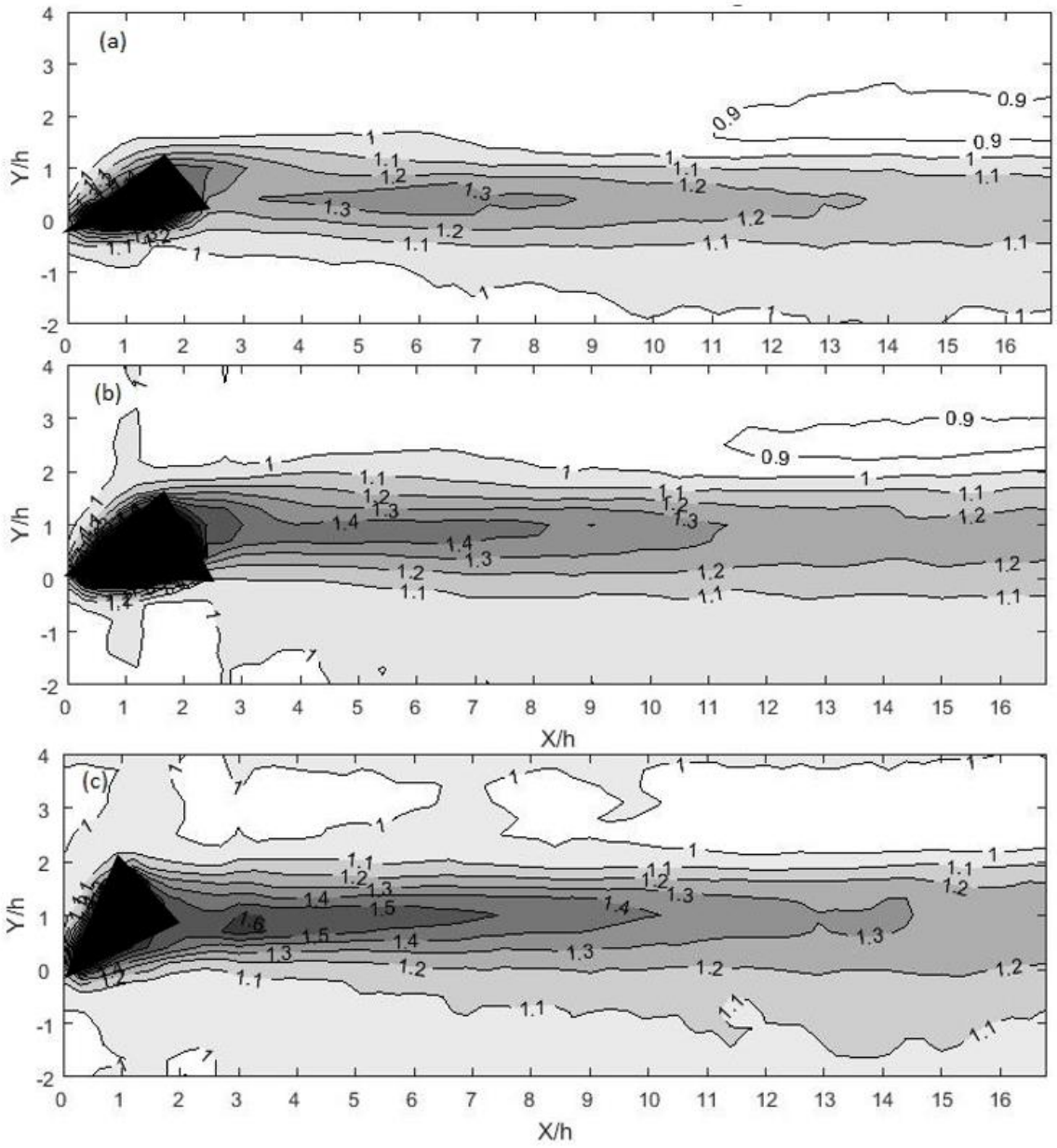

Figure 3. 3 The effect of inclination angle (a) 60° (b) 90° and (c) 120° on Nu/Nu_0 distribution.

To take a closer look at the convective heat transfer enhancement, the normalized Nusselt profile in the cross-sectional (Y) direction and how it evolves with distance downstream are plotted in Fig. 3.4. It is clear from the figure that the largest Nu/Nu_0 peak is produced by the 120-degree inclination angle delta winglet, and this peak value decreases as we move downstream (i.e. $Nu/Nu_0 \approx 1.65$, 1.48, and 1.31 at X/h = 3, 8, and 13, respectively). At X/h = 3, the location of the Nu/Nu_0 maximum hovers around Y/h = 1 for all three studied inclination angles. Farther downstream, the decaying Nu/Nu_0 peaks of the three inclination angles appear to depart from each other. The $\alpha = 120°$ maximum shifts slightly to the right (increasing Y/h), the $\alpha = 90°$ peak remains at $Y/h \approx 1$, and the $\alpha = 60°$ maximum moves to the left.

To the right of the peak, Nu/Nu_0 decreases to its minimum. This is true for all three studied β, where Nu/Nu_0 minimum occurs at $Y/h \approx 2\sim3$. These Nu/Nu_0 maximum and minimum were also detected by Nandana and Janoske [21]. The location of the Nu/Nu_0 minimum has been associated with the outflow region where there is a lack of fresh cold air from the freestream [22]. The fluid mechanics behind the thermal behavior of the current study will be expounded in the next section, where the flow details are delineated. It is interesting to note that the Nu/Nu_0 values to the left of the peak are higher than those to its right. These left-side values notably increase, while the right-side values decrease, with distance downstream. These seem to portray some history effect as the vortex street swirls downstream, picking up thermal energy along the way, in addition to the slow weakening of the vortex street. The enhanced area becomes larger as the downstream distance increases when considering the location where $Nu/Nu_0 \geq 1$, which can be

explained in terms of the expansion of the vortex. Also, the delta winglet with 120° inclination angle has the largest enhancement area.

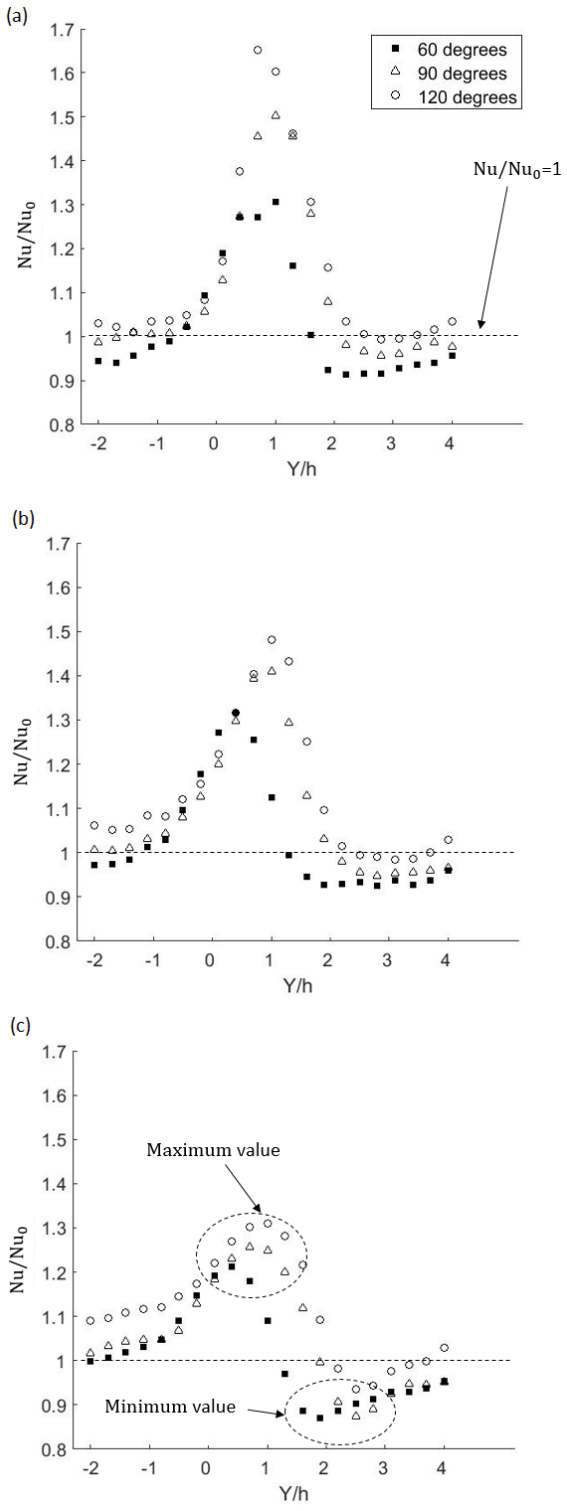

Figure 3. 4 The effect of the inclination angle (60°, 90°, 120°) on the cross-sectional Nu/Nu_0 profile at (a) X = 3h, (b) X = 8h, (c) X = 13h.

Figure 3.5 depicts the summit and valley values of normalized Nusselt numbers in the Y span direction with respect to distance downstream. The 120°-inclination angle winglet gave the largest maximum and minimum values in all the locations downstream, while the 60° winglet produced the lowest enhancement values. The value of maximum Nusselt numbers peak at the near wake region for the 120° and 90° inclination angles. In general, the summit value decreases with distance downstream. However, there appears to be an initial sharp decrease in the very near wake, which presumably has something to do with the 'heat fin effect' caused by the highly conductive aluminum winglet. Otherwise, the peak Nu/Nu_0 value increases with downstream distance, before it decreases farther downstream. This increasing followed by decreasing trend is more obvious at lower inclination angles. The decrease in the peak Nu/Nu_0 value for X/h larger than about 7 is probably due to the decay of the longitude vortex, the associated turbulence dissipation, and slight warming as the vortex picks up heat and swirls downstream. The valley (minimum) value of Nu/Nu_0 also has an overall (albeit slow) decrease with respect to downstream distance. It is interesting to note that this valley Nu/Nu_0 continues to drop below unity, even though the vortex street weakens. This less-than-no-winglet reference heat transfer rate appears to confirm the warming of the vortex street as it swirls downstream.

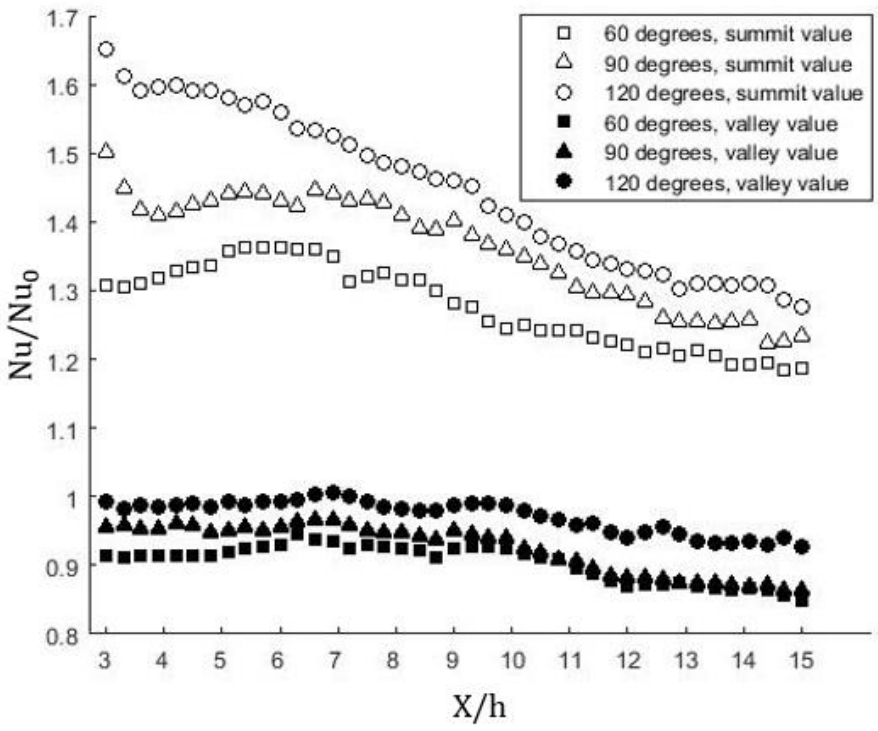

Figure 3. 5 The summit and valley Nu/Nu_0 in the Y direction with respect to downstream distance.

To evaluate the overall convective heat transfer performance, the average of Nu/Nu_0 in the Y direction is presented in Fig. 3.6. Two averages have been applied, one from Y/h = 0 (approximately the start of notable enhancement) to Y/h=1 (roughly the Nu/Nu_0 peak), see Fig. 4a, and the other from Y/h = -2 to 2 (the span over which notable change in Nu/Nu_0 has been detected). The entire enhancement region of Nu/ Nu_0 is approximately from Y/h= -2 to 2, beyond which Nu/Nu_0 falls back to unity. Therefore the region from Y/h = -2 to 2 is chosen to represent the overall enhancement of the normalized Nusselt number. For the 120° inclination angle case, the average Nu/Nu_0 between Y/h = 0 to 1 follows a continual decreasing trend. This decrease has also been observed by Xu et

al. [9] and Biswas et al. [23], and may be attributed to the decay of the primarily longitudinal vortex street. The continual decrease is not observed for the 60° and 90° winglets, where there is an increase after an initial decrease, beyond which the continual decrease takes place. When the average is taken over a wider Y span, from Y/h = -2 to 2, the variation of the averaged Nu/Nu_0 with respect to distance downstream becomes less obvious. The overall augmentation of Nu/Nu_0 lasted over the entire studied stretch, up to X/h of 16. Comparing Fig. 3.6(a) with 3.6(b), we see that while the most significantly altered Nu with respect to the reference Nu_0 decays with distance downstream, the larger span (Y/h = -2 to 2) average shows the averaged enhancement in Nu/Nu_0 is longer lasting. In other words, the vortex street seems to expand and thus weakens as far as its largest local boosting of Nu/Nu_0 is concerned (Fig. 3.4). On the other hand, the expansion spreads the vortex onto a larger span and thus, the overall enhancement in Nu/Nu_0 diminishes significantly slower. It is worth emphasizing that the most consistent observation is that the 120° winglet is the most effective heat transfer promoter.

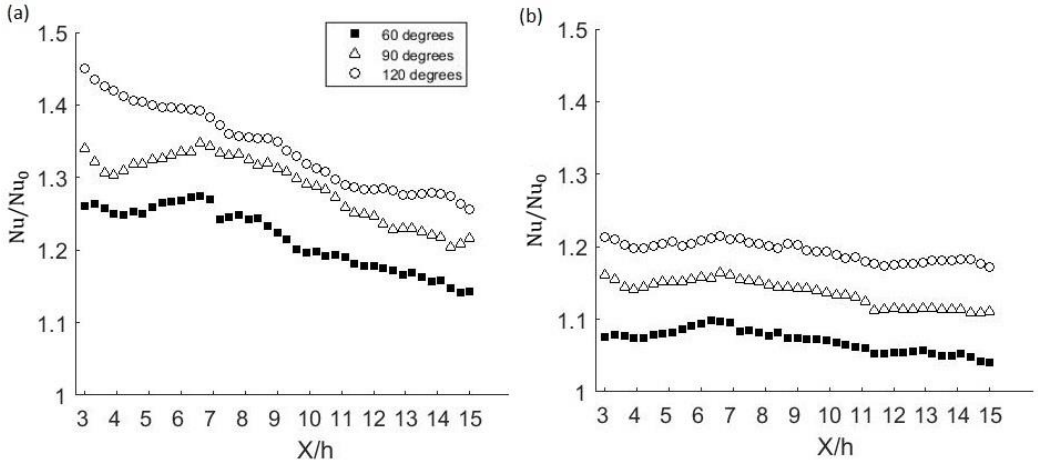

Figure 3. 6 Averaged Nu/Nu_0 with the respect to downstream distance (a) average between Y/h = 0 to 1, (b) average between Y/h = -2 to 2.

3.5.2 Flow Field

To understand the physics underlying the thermal performance observed, the flow field at X/h = 13 cross section was systematically scrutinized. To recognize the longitude vortex in the YZ plane, the cross-stream velocity vectors and non-dimensional vorticity are presented in Fig. 7. The uncertainty of the mean velocity is about 0.28m/s. The dotted lines in the figure show the delta winglet when looking upstream. A high vorticity region corresponds to the vortex. The region where the velocity vectors is pointing downward, into the heated surface, is called the "inflow region," while the region where the velocity vectors point away from the surface is termed the "outflow region." Cooler freestream air is brought to the hot surface in the inflow region and quickly sweeps to the right, and thus, the local convective heat transfer rate is notably enhanced. The flow to the right (looking upstream, as in Fig. 3.7) of the inflow region is dragged along the hot surface to the right. This heated air is subsequently scooped away from the surface by the outgoing flow in the outflow region. As this volume of air is saturated with thermal energy, it resulted in a local reduction in Nu; see Fig. 3.4.

The longitude vortex is bounded by the inflow and outflow regions. The highest vorticity region, consisting of the streamlines formed from the leading edge of the winglet, is the vortex core [24]. Other than the main vortex, smaller vortices induced by the main vortex are also detected. The location of the main vortex moves to the right, in the positive Y direction, as the inclination angle increases. This corroborates well with the local Nu/Nu_0 results shown in Fig. 3.4c, where the peak Nu/Nu_o occurs in the proximity of the inflow and just beneath the sweeping vortex core.

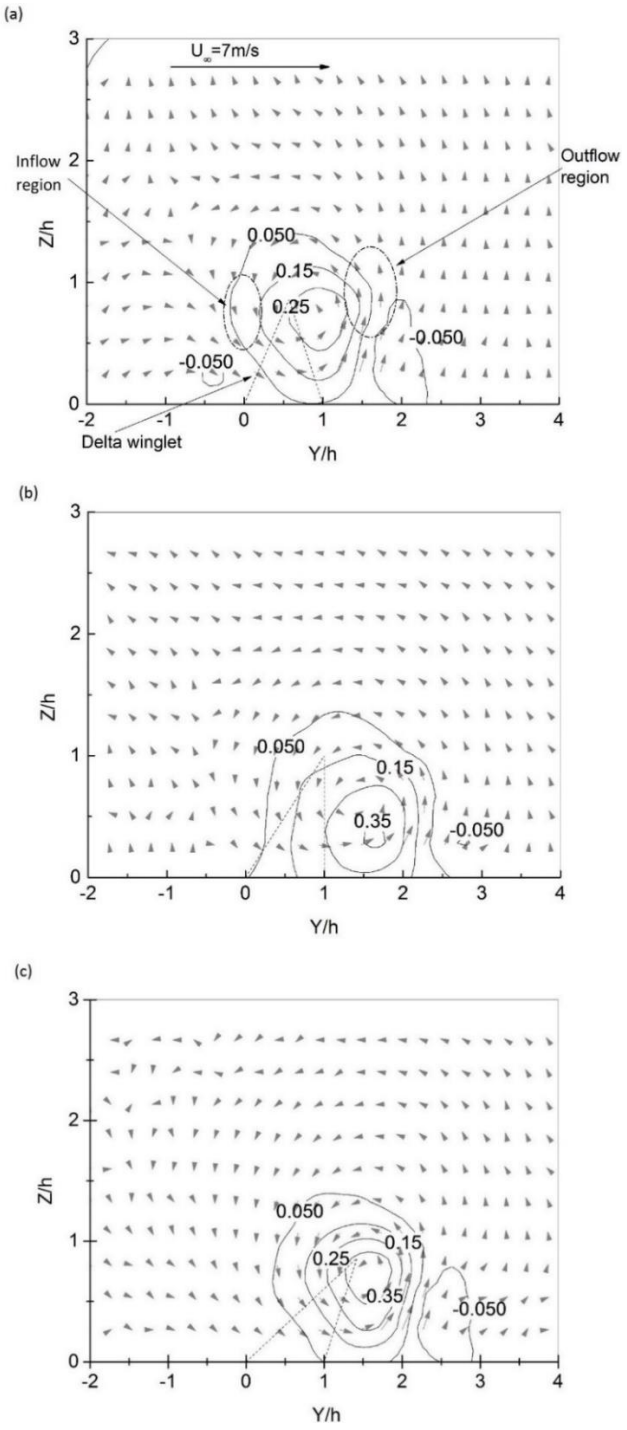

Figure 3. 7 Velocity vectors in the YZ plane and cross-stream non-dimensional vorticity (*Ω*) contours at 13h (200mm) downstream, (a) β = 60°, (b) β = 90°, (c) β = 120° .

The inflow and outflow regions can also be inferred from the average W (vertical) velocity within the boundary layer ($Z/h \leq 2$); see Figs. 3.8 and 3.9. As expected, the largest into-the-plate velocity coincides with the inflow region, while the largest out-of-plate velocity correlates to the outflow region. These locations also substantiate the peak and valley of Nu/Nu_0 depicted in Fig. 3.4c, with the peak corresponding roughly to the switching from negative W into a positive one. The inflow region moves to the right, in the positive Y direction, by approximately 0.53h (8mm) as the inclination angle increases from 60° to 120°. The into-the-plate velocity in the inflow region is the largest when the inclination angle is 120°, implying that the largest amount cool air is brought down to the surface, and quickly swept to the right, into the outflow. As such, the location of the inflow to sweeping region supports the largest peak Nu/Nu_0 value shown in Fig. 3.4.

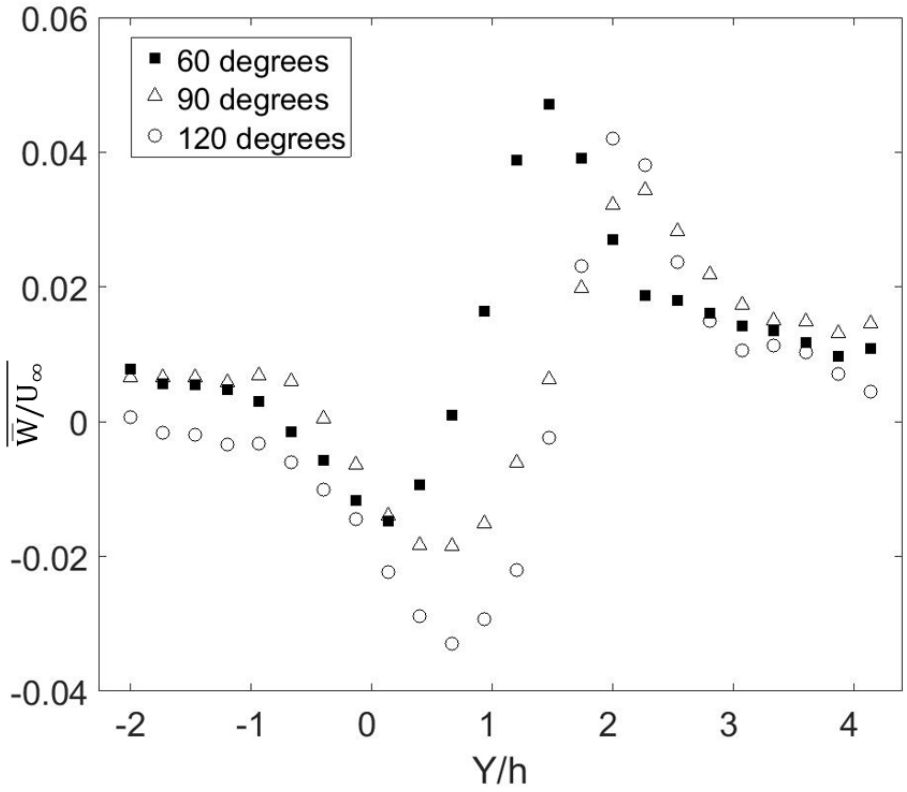

Figure 3. 8 $\overline{W}/U_\infty$, averaged from Z/h ≈ 0.2 to 2, versus Y/h.

To further elucidate the flow field, the boundary layer and velocity vectors are plotted in Fig. 3.9. It is clear from the figure that the vortical flow significantly distorted the flow field, including the boundary layer. The inner boundary layer where $\overline{U}/U_\infty \leq 0.95$ is squashed by the longitude vortex in the inflow region and extended away from the surface in the outflow region. These characteristics have also been observed by Hernon and Patten [25]. As a consequence, the thermal resistance of the inflow region is reduced while that in the outflow region is increased, as far as the boundary layer thickness is concerned. In agreement with Nu/Nu_o and $\overline{W}/U_\infty$ results, the swirling effect on the boundary is most significant when the inclination angle is 120°. Also

interesting to note is that the flow has the lowest near-surface stream-wise velocity when the inclination angle is 90°. This is because the winglet at this inclination angle poses the largest blockage. The thickness of the boundary hovered around 2.2h when β = 60° and 90°. The outflow region boundary layer is thickened to over 3h when β = 120°. It is thus clear that there is more to consider regarding the flow characteristics than the boundary layer thickness alone. In other words, the larger $\overline{W}/U_\infty$ induced by the β = 120° winglet seems to slightly offset the largest thermal resistance caused by this thickest boundary layer. Resultantly, the local Nu/Nu_o associated with the β = 120° winglet at the thickened boundary layer region remained higher than those of β = 60° and 90°, compare Fig. 3.9 with Fig. 3.4.

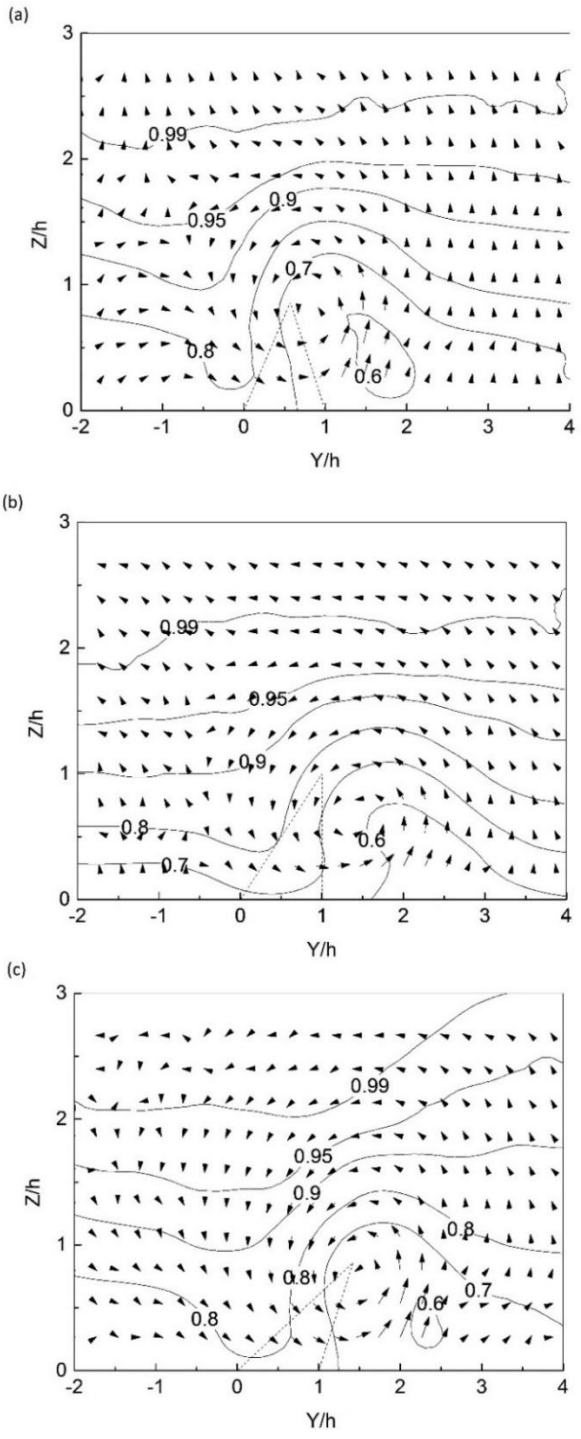

Figure 3. 9 Velocity vectors in YZ plane and stream-wise time-averaged velocity contours normalized by U_∞ (7m/s) at 13h (200mm) downstream, (a) β = 60°, (b) β = 90°, (c) β = 120°.

It is known that the convective heat transfer rate is directly related to the level of local turbulence. The average near-wall turbulent kinetic energy within the boundary layer ($Z/h \leq 2$) is depicted in Fig. 3.10. In general, the squashing in the inflow region drastically lowered the local turbulence intensity, while the cross-stream sweeping (to the right) and out-of-plate flow produced the most turbulence. The delta winglet with β = 90°, which has the largest blockage, resulted in marginally higher peak turbulence level than β = 120° at X/h = 13. More importantly, the peak turbulence intensity value consistently coincides with the peak Nu/Nu_o location in Fig. 3.4. Note that the uncertainty of k is around 5×10^{-3}, see appendix.

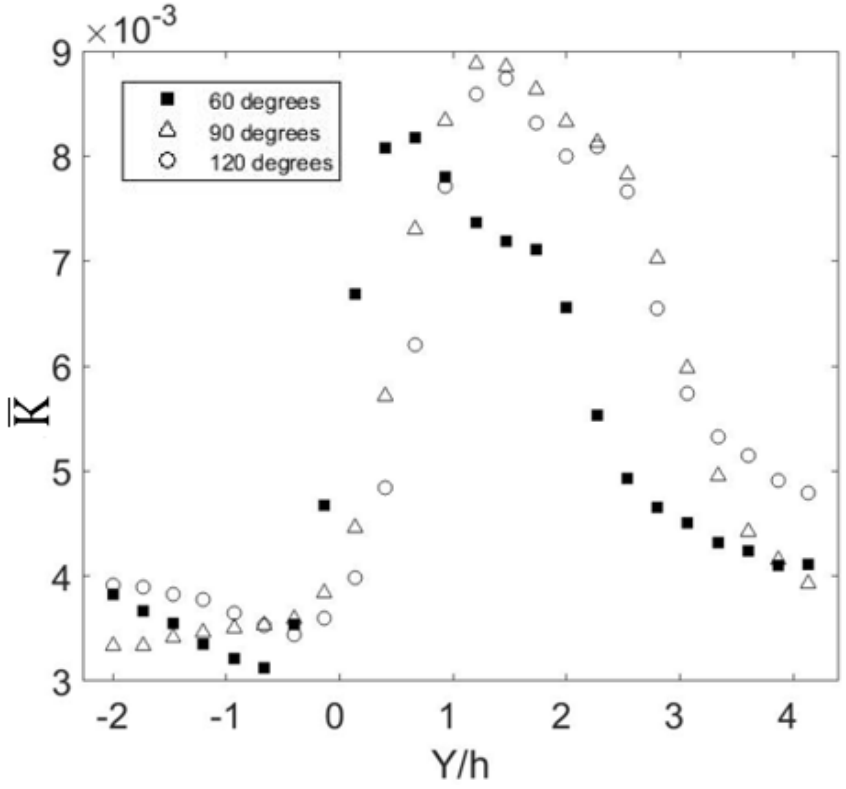

Figure 3. 10 Average of turbulent kinetic energy ($Z/h \leq 2$) in the Y direction at X = 13h.

3.6 Conclusion

The effect of the inclination angle (β = 60°, 90°, 120°) of a delta winglet with an aspect ratio (c/h) of 2 on the convection heat transfer enhancement from a heated flat plate has been experimentally studied at Re_h of 6300. The winglet with β = 120° was found to consistently give the highest heat transfer enhancement. This is clearly depicted in terms of the largest peak and overall Nu/Nu_o across ±2h cross section, up to 16h downstream (i.e. over the entire studied stretch of the heated plate). Detailed flow characterization revealed the inflow, where cooler freestream air was brought onto the hot plate, as the main driver in substantially increasing the local Nu/Nu_o. The peak Nu/Nu_o corresponds to the inflow region, where the cooler freestream air brought toward the surface is being swept across the hot surface. The β = 120° winglet, which produced the most intense inflow with the largest into-the-plate velocity component, also generated the highest overall turbulence level, though the peak turbulence level is just shy of that corresponding to the β = 90° case, which has the highest stream-wise blockage. The winglet with β = 60° resulted in the least amount of heat transfer enhancement among the three studied inclination angles.

Acknowledgement

This work was made possible by Natural Sciences and Engineering Research Council of Canada and Ontario Centres of Excellence.

References

[1] Jindal, P., Agarwal, S., Sharma, R. P., and Roy, A. K., 2018, "Enhancement of Film Cooling Effectiveness Using Rectangular Winglet Pair," Journal of Thermal Science and Engineering Applications, **10**(4), pp. 041014-041014–9.

[2] Agarwal, S., and Sharma, R. P., 2016, "Numerical Investigation of Heat Transfer Enhancement Using Hybrid Vortex Generator Arrays in Fin-and-Tube Heat Exchangers," Journal of Thermal Science and Engineering Applications, **8**(3), pp. 031007-031007–9.

[3] Awais, M., and Bhuiyan, A. A., 2018, "Heat Transfer Enhancement Using Different Types of Vortex Generators (VGs): A Review on Experimental and Numerical Activities," Thermal Science and Engineering Progress, **5**, pp. 524–545.

[4] Eibeck, P., and Eaton, J., 1987, "Heat Transfer Effects of a Longitudinal Vortex Embedded in a Turbulent Boundary Layer," Journal of Heat Transfer, **109**(1), pp. 16–24.

[5] Pal, A., Bandyopadhyay, D., Biswas, G., and Eswaran, V., 2012, "Enhancement of Heat Transfer Using Delta-Winglet Type Vortex Generators with a Common-Flow-up Arrangement," Numerical Heat Transfer, Part A: Applications, **61**(12), pp. 912–928.

[6] Khanoknaiyakarn, C., Promvonge, P., Thianpong, C., and Skullong, S., 2018, "Performance Improvement in a Tubular Heat Exchanger by Punched Delta-Winglet Vortex Generators," IOP Conference Series: Materials Science and Engineering, IOP Publishing, p. 012068.

[7] Li, W., Khan, T. A., Tang, W., and Minkowycz, W., 2018, "Numerical Study and Optimization of Corrugation Height and Angle of Attack of Vortex Generator in

the Wavy Fin-and-Tube Heat Exchanger," Journal of Heat Transfer, **140**(11), p. 111801.

[8] Liang, G., Islam, M., Kharoua, N., and Simmons, R., 2018, "Numerical Study of Heat Transfer and Flow Behavior in a Circular Tube Fitted with Varying Arrays of Winglet Vortex Generators," International Journal of Thermal Sciences, **134**, pp. 54–65.

[9] Xu, Y., Islam, M., and Kharoua, N., 2018, "Experimental Study of Thermal Performance and Flow Behaviour with Winglet Vortex Generators in a Circular Tube," Applied Thermal Engineering, 135, pp. 257–268.

[10] Syaiful, Y., B., Saryanto, A., and Bae, M.-W., 2018, "Pressure Loss Penalty Improvement of Airflow through Heated Plate Mounted by Delta Winglet Vortex Generator: An Experimental Study," *AIP Conference Proceedings*, AIP Publishing, p. 020033.

[11] Khan, T. A., and Li, W., 2018, "Optimal Configuration of Vortex Generator for Heat Transfer Enhancement in a Plate-Fin Channel," Journal of Thermal Science and Engineering Applications, **10**(2), p. 021013.

[12] Wu, H., Ting, D. S.-K., and Ray, S., 2018, "The Effect of Delta Winglet Attack Angle on the Heat Transfer Performance of a Flat Surface," International Journal of Heat and Mass Transfer, **120**, pp. 117–126.

[13] Lei, Y.-G., He, Y.-L., Tian, L.-T., Chu, P., and Tao, W.-Q., 2010, "Hydrodynamics and Heat Transfer Characteristics of a Novel Heat Exchanger with Delta-Winglet Vortex Generators," Chemical Engineering Science, **65**(5), pp. 1551–1562.

[14] Oneissi, M., Habchi, C., Russeil, S., Bougeard, D., and Lemenand, T., 2016, "Novel Design of Delta Winglet Pair Vortex Generator for Heat Transfer Enhancement," International Journal of Thermal Sciences, **109**, pp. 1–9.

[15] Ghahfarokhi, P. S., Kallaste, A., Vaimann, T., and Belahcen, A., 2018, "Natural Convection from Flat Side's of Coil System," *2018 19th International Scientific Conference on Electric Power Engineering (EPE)*, IEEE.

[16] He, J., Liu, L., and Jacobi, A. M., 2010, "Air-Side Heat-Transfer Enhancement by a New Winglet-Type Vortex Generator Array in a Plain-Fin Round-Tube Heat Exchanger," Journal of Heat Transfer, **132**(7), pp. 071801-071801–9.

[17] Jørgensen, F. E., 2005, "*How to Measure Turbulence with Hot-Wire Anemometers: A Practical Guide*, Dantec dynamics.

[18] Ting, D. S-K., 2016, Basics of Engineering Turbulence, Academic Press, New York.

[19] Figliola, R. S., and Beasley, D. E., 2001, Theory and Design for Mechanical Measurements, IOP Publishing.

[20] Wang, Y., He, Y.-L., Yang, W.-W., and Cheng, Z.-D., 2015, "Numerical Analysis of Flow Resistance and Heat Transfer in a Channel with Delta Winglets under

Laminar Pulsating Flow," International Journal of Heat and Mass Transfer, **82**, pp. 51–65.

[21] Nandana, V., and Janoske, U., 2018, "Numerical Study on the Enhancement of Heat Transfer Performance in a Rectangular Duct with New Winglet Shapes," Thermal Science and Engineering Progress, **6**, pp. 95–103.

[22] Luo, L., Wen, F., Wang, L., Sundén, B., and Wang, S., 2017, "On the Solar Receiver Thermal Enhancement by Using the Dimple Combined with Delta Winglet Vortex Generator," Applied Thermal Engineering, **111**, pp. 586–598.

[23] Biswas, G., Chattopadhyay, H., and Sinha, A., 2012, "Augmentation of Heat Transfer by Creation of Streamwise Longitudinal Vortices Using Vortex Generators," Heat Transfer Engineering, **33**(4–5), pp. 406–424.

[24] Herpe, J., Bougeard, D., Russeil, S., and Baudoin, B., 2006, "Numerical Investigation of Entropy Generation in the Case of a Finned Oval Tube With a Punched Longitudinal Vortex Generator in Form of Delta Winglet," *ASME 2006 2nd Joint US-European Fluids Engineering Summer Meeting Collocated With the 14th International Conference on Nuclear Engineering*, American Society of Mechanical Engineers, pp. 1037–1046.

[25] Hernon, D., and Patten, N., 2009, "Hotwire Measurements Downstream of a Delta Winglet Pair at Two Angles of Attack," *ASME 2009 Heat Transfer Summer Conference Collocated with the InterPACK09 and 3rd Energy Sustainability Conferences*, American Society of Mechanical Engineers, pp. 777–784.

CHAPTER 4

CONCLUSIONS

4.1 Summary and conclusions

Delta winglet is a promising turbulent generator which can generate longitude vortex superimposed on the high-intensity turbulence to enhance the convective heat transfer rate. The delta winglet can be applied on the solar panel to lower the cell temperature of the PV solar panel to improve its efficiency.

In chapter 2, the role of the inclination angle $\beta = 90° \,\&\, 120°$ of a *c/h* = 2 (*c* = winglet chord length, h = winglet height) delta winglet at 30° with respect to a Re_h = 9000 wind was experimentally investigated. The vortical flow is quantified in terms of vortex size, vorticity, turbulence intensity, integral length, and Taylor microscale. The boundary layer is found to be progressively disturbed as the vortical flow-boundary layer interactions evolve. As the inclination angle increases, the longitudinal vortex reduces and shifts toward the outflow side. Along with the shrinking of the longitudinal vortex is a reduced turbulent boundary layer. Moreover, with an increasing inclination angle, the into-the-plate velocity in the inflow region increases, but the corresponding out-of-plane velocity in the outflow region decreases. The perturbed flow field turbulence is also lowered when increasing β from 90° to 120°.

The effect of the inclination angle (β = 60°, 90°, 120°) of a delta winglet with an aspect ratio (c/h) of 2 on the convection heat transfer enhancement from a heated flat plate has been experimentally studied at Re_h of 6300 in chapter 3. In this chapter, the winglet with β = 120° is found to consistently give the highest heat transfer enhancement, which is

depicted in terms of the largest peak and overall Nu/Nu_o across ±2h cross-section, up to 16h downstream (i.e., over the entire studied stretch of the heated plate. The peak Nu/Nu_o corresponds to the inflow region, where the cooler freestream air brought toward the surface is being swept across the hot surface. The $\beta = 120°$ winglet produced the most the largest into-the-plate velocity component, also generated the highest overall turbulence level, though the peak turbulence level is just shy of that corresponding to the $\beta = 90°$ case, which has the highest stream-wise blockage. The winglet with $\beta = 60°$ resulted in the least amount of heat transfer enhancement among the three studied inclination angles.

4.2 Recommendations

Based on the results of the current study, the delta winglet can generate the longitude vortex in the flow. Also, the inclination angle of 120 degrees can effectively enhance the heat transfer rate. However, there are still some problems if we want to apply our work to the solar panel.

All the results are shown in non–dimensional form. The height of the delta winglet, h=15mm, is used to normalize the distance. In the experiment, the enhancement lasts the entire length of heated plate, 16h or 240 mm. Dimensionally, this implies that for a 1 m long solar panel, a 60 mm high winglet is neede-d.

More work needs to be done to fully understand the mechanism of the heat transfer rate and the flow characteristics. And more experiments need to be done on the winglet. In the thesis, only three inclination angles of delta winglet were studied. So, to make the conclusion more convincing, more inclination angles of delta winglet such as 130 degrees,

135 degrees or 140 degrees need to be investigated. Moreover, the optimum attack angle and aspect ratio of the delta winglet for 120 degrees may be another good direction to study. Furthermore, in order to apply the winglet to a larger plane, the delta winglet pair with an inclination angle of 120 degrees needs to be explored.

APPENDICES

Appendix A Uncertainty Analysis

The total uncertainty (E) in the current study of each parameter comes from the uncertainty of bias (B) and the precision (P) which comes from the process of acquiring the instantaneous velocity data. The uncertainty of $\overline{U}$ can be deduced from:

$$E = \sqrt{B^2 + P^2} \tag{A-1}$$

Uncertainty of U_i

For a typical point at Y/h=0 and Z/h=1.5, the bias uncertainty of instantaneous velocity comes from the process of calibration (0.194 m/s), linearization (0.097 m/s), A/D resolution (0.078 m/s) and probe positioning (0.015 m/s). Therefore, the bias uncertainty of the instantaneous velocities is:

$$B(U_i) = \sqrt{0.194^2 + 0.097^2 + 0.0776^2 + 0.01455^2} = 0.2\ \mathrm{m/s} \tag{A-2}$$

The precision of the instantaneous velocity is estimated by resetting the hotwire to the freestream and measuring the velocity for 20 times. For each measurement, N = 10^6 points were measured. P follows the Student's t distribution method with a 95% confidence interval (choose repeat time M is 2×10^7, so t value is 1.960).

$$P(U_i) = 0.11\ \mathrm{m/s} \tag{A-3}$$

So the total uncertainty of U_i is:

$$E(U_i) = \sqrt{B(U_i)^2 + P(U_i)^2} = 0.23\mathrm{m/s} \tag{A-4}$$

Uncertainty of $\overline{U}$

The mean velocity (7m/s) bias uncertainty can be estimated as:

$$B(\overline{U}) = B(U_i) = \ 0.20\ m/s \tag{A-5}$$

The precision uncertainty of the mean velocity is estimated by resetting the hotwire to the typical position and measuring the velocity for 20 times. So, t is 2.08.

The precision of the $\overline{U}$ can be expressed as:

$$\mathrm{P}(\overline{U}) = 0.20\ \mathrm{m/s} \tag{A-6}$$

So, the uncertainty of $\overline{U}$ is:

$$E(\overline{U}) = \sqrt{B(\overline{U})^2 + P(\overline{U})^2} = 0.28\ \mathrm{m/s} \tag{A-7}$$

Uncertainty of u_{rms}

The corresponding bias uncertainty in u_{rms} (0.345m/s) can be estimated as:

$$\mathrm{B}(u_{rms}) = 0.01035 m/s \tag{A-8}$$

The precision of the u_{rms} is obtained from 20 measurement of the typical point, which is:

$$\mathrm{P}(u_{rms}) = 0.028 m/s \tag{A-9}$$

So the uncertainty of u_{rms} is:

$$\mathrm{E}(u_{rms}) = \sqrt{B(u_{rms})^2 + P(u_{rms})^2} = 0.029\ \mathrm{m/s} \tag{A-10}$$

Heat transfer

The temperature captured by the thermal camera is calibrated by the thermal couple which has a bias uncertainty of 0.5 ℃. And the temperature at the top surface is captured 10 times by the thermal camera, which leads to a precision uncertainty of 0.36℃. The uncertainty of each parameter associated with heat transfer can be deduced by the propagation of the uncertainty:

$$E(Q_{total}) = \sqrt{[\frac{\partial Q_{total} E(T_{top})}{\partial T_{top}}]^2} = \frac{K_{PTFE} A}{t_{PTFE}} E(T_{top}) \quad \text{(A-10)}$$

$$E(Q_{radiation}) = \sqrt{[\frac{\partial Q_{radiation} E(T_{top})}{\partial T_{top}}]^2} = 4\varepsilon\sigma A T_{top}^3 E(T_{top}) \quad \text{(A-11)}$$

$$E(Q_{convection}) = \sqrt{[\frac{\partial Q_{convection} E(Q_{total})}{\partial Q_{total}}]^2 + [\frac{\partial Q_{convection} E(Q_{radiation})}{\partial Q_{radiation}}]^2} \quad \text{(A-12)}$$

$$= \sqrt{[E(Q_{total})]^2 + [E(Q_{radiation})]^2}$$

$$E(h) = \sqrt{[\frac{\partial h E(Q_{convection})}{\partial Q_{convection}}]^2 + [\frac{\partial h E(T_{top})}{\partial T_{top}}]^2} \quad \text{(A-13)}$$

$$= \sqrt{[\frac{E(Q_{convection})}{A(T_{top} - T_{air})}]^2 + [\frac{Q_{convection} E(T_{top})}{A(T_{top} - T_{air})^2}]^2}$$

$$E\left(\frac{Nu}{Nu_0}\right) = \sqrt{[\frac{\partial \frac{Nu}{Nu_0} E(h)}{\partial h}]^2 + [\frac{\partial \frac{Nu}{Nu_0} E(h_0)}{\partial h_0}]^2} = \sqrt{[\frac{E(h)}{h_0}]^2 + [\frac{h E(h_0)}{{h_0}^2}]^2} \quad \text{(A-14)}$$

$$= 0.06$$

The uncertainty of normalized Nusselt number is 0.06, which is similar to a typical individual enhancement. When looking at the average Nu/ Nu0, it can be found that all of the enhancement in the downstream region are larger than 0.06. Moreover, the enhancement is consistently observed throughout, including in the various average. Therefore, the observed enhancement is definite.

Appendix B The Effect of Reynolds Number on Heat Transfer

The effect of Reynolds number on heat transfer augmentation was examined in this part. Two Reynolds number was presented in this section one is $Re_h \approx 9000$ (U_∞=10 m/s) and another one is $Re_h \approx 6300$ (U_∞ = 7 m/s). The winglet was the same as described in Chapter 4. The inclination angle of the winglet is chosen to 120 degrees.

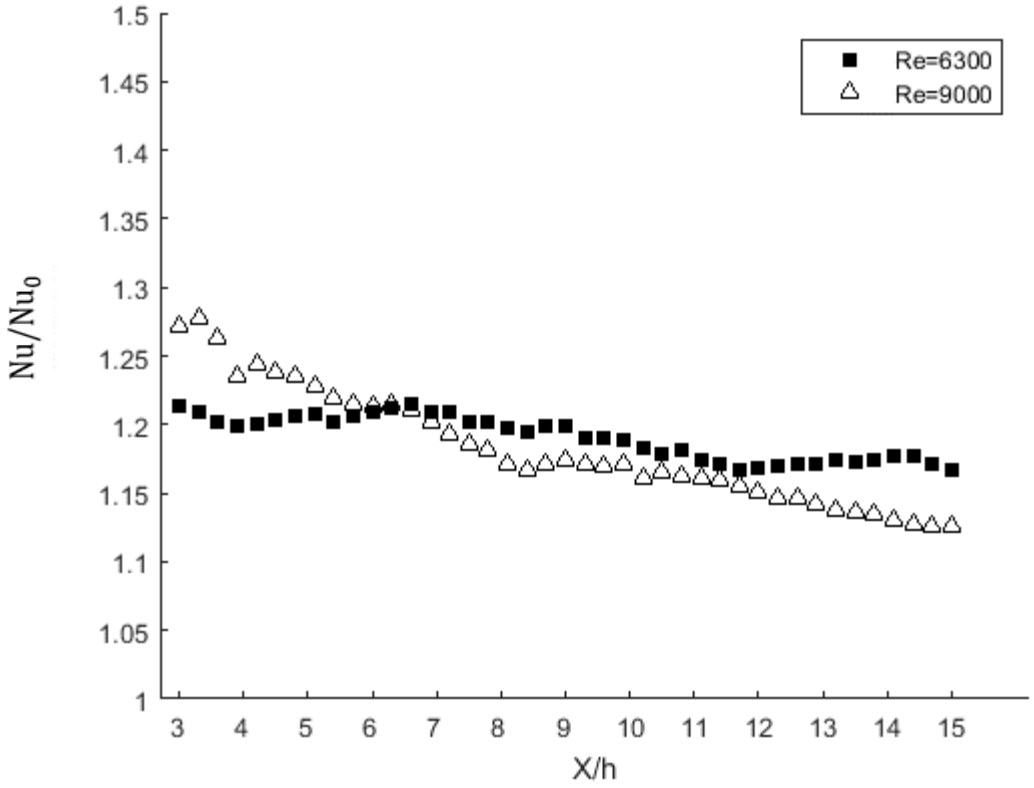

Figure B. 1 Averaged Nu/Nu_0 with the respect to downstream distance average between Y/h = -2 to 2

To evaluate the overall convective heat transfer performance, the average of Nu/Nu_0 in the Y direction is presented in Fig. B.1. The average is from Y/h = -2 to 2. For both cases, the average Nu/Nu_0 between Y/h = -2 to 2 follows a continual decreasing trend.

The average Nu/Nu_0 when $Re_h \approx 9000$ is higher at initial. However, in the further downstream region, the enhancement is larger when $Re_h \approx 6300$.

Appendix C Efficiency Enhancement Analysis

The relationship between the cell temperature of the solar panel and the efficiency of the PV panel can be calculated from:

$$\eta = \eta_{ref}[1 - \beta(T_C - T_{ref})] \quad \text{(C-1)}$$

To evaluate the efficiency enhancement, the average efficiency with the delta winglet of the solar panel was normalized by the efficiency for the no winglet case, i.e.,

$$\frac{\eta}{\eta_0} = \frac{1 - \beta(T_C - T_{ref})}{1 - \beta(T_{C,0} - T_{ref})} \quad \text{(C-2)}$$

T_C is the cell temperature which can be deduced from the upper surface temperature of the PTFE plate measured by the thermal camera. T_{ref} is the reference temperature of the solar which is 25℃. The temperature coefficient β is 0.0041. The average T_C of the upper surface for the downstream distance from X/h= 3 to 13 and for Y span from Y/h= 0 to 1 is 63.6℃. On the other hand, the average temperature $T_{C,0}$ of the panel without the winglet for the same area is 69.1℃. Based on the calculation, the enhancement value of the efficiency is 1.03.

Appendix D Heat transfer enhancement with different inclination angle from 30 to 150 degrees

Figure D.1 show the normalized Nusselt numbers from 30 to 150 degrees' inclination angle of delta winglet which are averaged from Y/h = -2 to 2 and X/h = 3 to 16. The largest enhancement of the convective heat transfer rate caused by the delta winglet occurs when the inclination angle is 120 degrees. And the enhancement is lowest when the inclination angle is 60 degrees and 150 degrees.

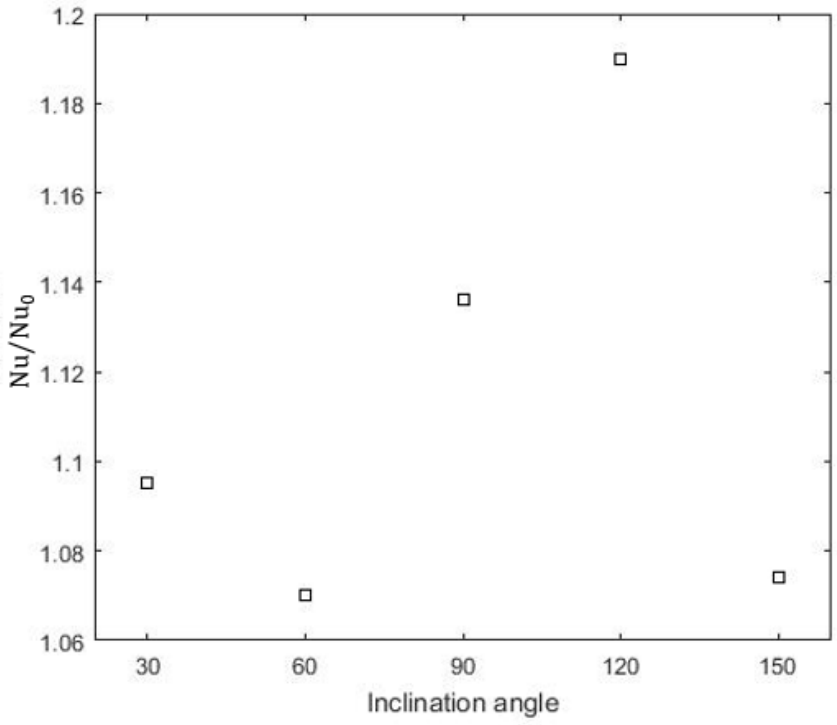

Figure D. 1 Normalized Nusselt numbers averaged from Y/h = -2 to Y/h = 2 and X/h from 3 to 16 for with inclination angle from 30 to 150 degrees.

Appendix E Paper Publication Status

Junguo Wang[1], David S-K. Ting[1], Steve Ray[2]

[1]*Turbulence and Energy Laboratory, Center for Engineering Innovation, University of Windsor,*

401 Sunset Ave, Windsor, Ontario, N9B 3PP4, Canada

[2]*Essex Energy Corporation, 2199 Blackacre Dr, Suit#2, Oldcastle, Ontario, N0R 1L0, Canada*

Wang, J., Ting, D. S.-K., and Ray, S., 2018, "The Effect of Delta Winglet Inclination Angle on the Vortical Flow Downstream," *ASME 2018 IMECE*, American Society of Mechanical Engineers, p. V007T09A026–V007T09A026.

Wang, J., Ting, D. S.-K., and Ray, S., "The Role of delta winglet inclination angle on Heat Transfer Enhancement," *ASME Journal of Thermal Science and Engineering Applications*, under review.

VITA AUCTORIS

NAME:	Junguo Wang
PLACE OF BIRTH:	Shenyang, Liaoning, China
YEAR OF BIRTH:	1993
EDUCATION:	Tieling High School, Tieling, Liaoning, 2009
	Tianjin University, B.Sc., Tianjin, China, 2012
	University of Windsor, M.Sc., Windsor, ON, 2017